Exp Fluids (2014) 55:1773
DOI 10.1007/s00348-014-1773-x

REVIEW ARTICLE

Frictional drag reduction by bubble injection

Yuichi Murai

Received: 8 February 2014 / Revised: 15 June 2014 / Accepted: 17 June 2014 / Published online: 15 July 2014

Abstract The injection of gas bubbles into a turbulent boundary layer of a liquid phase has multiple different impacts on the original flow structure. Frictional drag reduction is a phenomenon resulting from their combined effects. This explains why a number of different void–drag reduction relationships have been reported to date, while early works pursued a simple universal mechanism. In the last 15 years, a series of precisely designed experimentations has led to the conclusion that the frictional drag reduction by bubble injection has multiple manifestations dependent on bubble size and flow speed. The phenomena are classified into several regimes of two-phase interaction mechanisms. Each regime has inherent physics of bubbly liquid, highlighted by keywords such as bubbly mixture rheology, the spectral response of bubbles in turbulence, buoyancy-dominated bubble behavior, and gas cavity breakup. Among the regimes, bubbles in some selected situations lose the drag reduction effect owing to extra momentum transfer promoted by their active motions. This separates engineers into two communities: those studying small bubbles for high-speed flow applications and those studying large bubbles for low-speed flow applications. This article reviews the roles of bubbles in drag reduction, which have been revealed from fundamental studies of simplified flow geometries and from development of measurement techniques that resolve the inner layer structure of bubble-mixed turbulent boundary layers.

Y. Murai (✉)
Laboratory for Flow Control, Division of Energy and Environmental Systems, Faculty of Engineering, Hokkaido University, N13W8, Sapporo 060-8628, Japan
e-mail: murai@eng.hokudai.ac.jp

1 Introduction

The use of bubbles as a way of reducing skin frictional drag in turbulent flows has long been a focus for engineers in the expectation that it is applicable to ships and pipelines. The first success was reported in the literature more than 40 years ago: McCormick and Bhattacharyya (1973) employed electrolysis to generate microbubbles in water and were able to demonstrate a significant degree of drag reduction for a submersible hull. If gas films are included in this topic, we could further go back to the paper of Hirata and Nishiwaki (1963), who measured pressure loss in a horizontal channel flow containing gas in a film state. After the dawn of such technology, fluid engineering researchers began discussing the basic mechanism, which was conceptualized as a change in mixture properties such as the local average density and viscosity of the liquid containing bubbles. Legner (1984) suggested that shear thickening owing to an increase in local effective viscosity reduces wall shear stress. Marie (1987) explained the decrease in Reynolds shear stress with a local reduction in density. However, later experimental results did not parametrically support these hypotheses and rather indicated the difficulty of elucidating the correct perspective of the mechanism. On the one hand, this background encouraged full-dress laboratory research on a bubble-mixed boundary layer. A series of laboratory experiments using water channels and tunnels were conducted from the 1980s to 1990s, such as those of Madavan et al. (1985), Merkle and Deutsch (1990, 1992), and Kato et al. (1999). On the other hand, demands for practical use by vessels increased with changes in economical and environmental circumstances such as jumps in the oil price and the implementation of energy-saving strategies and international greenhouse gas regulations. Since 2000, activity relating to this topic came

to a hottest generation especially among maritime researchers, energetically challenging to reach a comprehensive understanding of the drag reduction toward practical use (Kodama et al. 2000; Moriguchi and Kato 2002). Experimentalists introduced state-of-the-art measurement instrumentations into quantitative monitoring of the boundary layer. They expanded measurement principles established for single-phase flow to allow investigation of bubbly two-phase flow, such as for laser Doppler velocimetry (LDV), particle image velocimetry (PIV), and ultrasonic velocity profiling. Numerical researchers computed the two-way interaction between turbulence and bubbles with direct numerical simulation (DNS)-like high-resolution schemes (Xu et al. 2002; Ferrante and Elghobashi 2004; Pang et al. 2013). Although their simulations were somewhat limited to sparse spherical bubbles, how bubbles attack surrounding turbulent eddies has been elucidated. They left us a significant scientific perspective of the drag reduction mechanism, and also helped interpret numerous past experimental data.

In the last decade, there has been great progress in both fundamental research and applications to industry. The progress was made possible by sophisticated measurement techniques for monitoring high-speed two-phase boundary layer flows (Kitagawa et al. 2005; Zhen and Hassan 2006; Murai et al. 2006a, b, c, 2009). Another impulse for the progress has been well-designed problem setting in research of multiphase fluid dynamics, such as the use of Taylor–Couette flow (van den Berg et al. 2005; Murai et al. 2008; van Gils et al. 2013). Furthermore, the lack of reproducibility in drag reduction, which has long been a concern among experimentalists, has come to the fore. We are now familiar with the concept that reproducibility is affected by contamination in water (Winkel et al. 2004; Takagi and Matsumoto 2011) and by naturally induced void waves that are generated by the bubble–drag time-lag mechanism (Murai et al. 2007; Park et al. 2009). The present article reviews the basic concept, history, and current discussion of bubble-induced drag reduction.

2 Drag reduction mechanism

Experimental correlation between the bubbling condition and resultant drag reduction explains little about the underlying physics of drag reduction. The causal relation comprises extremely complicated multivariable nonlinear functions. In fact, drag reduction mechanisms proposed by researchers diverge seriously, which is confusing when attempting to design their practical applications.

Table 1 lists the parameters we need to handle in experimentation for a single case of application. The target of interest is simply the wall shear stress, τ_w. Three primary parameters are managed to modify the wall shear stress: flow velocity U, gas flow rate Q, and mean bubble size d. The performance of drag reduction itself is evaluated

Table 1 List of parameters in drag reduction by bubble injection

Target parameters			
τ_w	Wall shear stress		
Apparent control parameters		Boundary layer characterizing scales	
U	Liquid flow velocity	δ	Boundary layer thickness
Q	Bubble volume flow rate	l	Wall unit
d	Bubble diameter	θ	Air cavity equivalent gas layer thickness
Environmental parameters			
P	Hydrostatic pressure		
g	Acceleration of gravity		
μ	Liquid viscosity		
ρ	Liquid density		

Code	Name	Description	Dominant in
Mechanism-governing dimensionless parameters			
Re	Reynolds number	Original flow structure	Single-phase flow
Fr	Froude number	Buoyancy effect	Air cavity and large bubble regime
We	Weber number	Inertia deformation	High turbulent regime
Ca	Capillary number	Viscous deformation	Bubbles smaller than coherent structure
Ma	Mach number	Compressibility	High-speed flow
α	Void fraction	Impact to liquid	All regimes

according to the correlation among these explicitly managed parameters. However, the internal physics of the boundary layer is highly difficult to deduce as it is described by so many parameters in the table; there are at least six dimensionless parameters involved when trying to solve the fluid dynamic mechanism. In this chapter, several important perspectives in reading the experimental results are offered, starting with the origin of the concept.

2.1 Fluid engineering basis

In general formulation, frictional drag is described by

$$D = C_f \cdot \frac{1}{2} \cdot \rho \cdot (U_w - U_f)^2 \cdot A, \quad (1)$$

where D, C_f, ρ, U_w, U_f, and A are the frictional drag, friction coefficient, density of fluid, velocity of the moving wall, velocity of the fluid outside the boundary layer, and area of fluid contact with the wall. In this aspect of fluid engineering, the equation tells us that the drag can be reduced when any of the five variables on the right-hand side of the equation is lowered. Apparently, reducing the relative velocity, $U_w - U_f$, realizes drag reduction with its squared impact, and this approach has been practically applied in shipping to save fuel consumption per unit distance (Ronen 1982). Without the deceleration of the moving wall, the injection of bubbles around the wall reduces the local average density of the fluid, ρ, and therefore reduces the drag. This is categorized as the inertia effect of drag reduction, which plays the major role in turbulent flow states (Marie 1987). Maintaining large bubbles close to the wall reduces A, the area of wall contact. A 100 % replacement of liquid phase with air phase within the boundary layer removes almost all the drag, and there only remains the friction of air, which is small enough compared with that of liquid. This replacement-based drag reduction is termed the air layer method (Sanders et al. 2006). If the gas layer forms a thin, but stable gas films at low shearing environment, it is termed the gas film method (Fukuda et al. 2000). These two methods can be categorized to the same approach in a broad sense and are commonly termed the gas layer method in this paper, while gas–liquid interface takes different structures inside the boundary layer. In contrast, there are techniques of producing and stabilizing gas cavity such as by installing a stepwise stern in the upstream region of the target wall. The stern separates main stream from the wall so that a relatively stagnant gas cavity is maintained in the vicinity of wall. This is termed the gas cavity method. The techniques rely on gravity and the geometry of the target body and were comprehensively reviewed by Ceccio (2010).

Summarizing above, we have to distinguish three primary types from gas supplying-based drag reduction techniques as illustrated in Fig. 1. (a) Bubble drag reduction (BDR) works with action of dispersed bubbles inside the boundary layer. (b) Gas layer drag reduction (GLDR) relies on replacement of highly shearing liquid with gas in the form of froths or long gas films. (c) Gas cavity drag reduction (GCDR) occurs when backward step provides a large gas single-phase space. Elbing et al. (2008) and their group (Sanders et al. 2006; Mäkiharju et al. 2013a, b) investigated the transition among these three types. By supplying air into water, they observed GLDR effect between BDR and GCDR in a spatially developing two-phase boundary layer. GLDR realizes with complex gas–liquid interfaces, but plays an important role in applications where spatially developing turbulent boundary layers are targeted such as for maritime vessels. Gas phase is unlimited to water and seawater, but can be any suitable gas for liquid pipeline applications, such as, nitrogen, hydrogen, carbon dioxide, and gaseous fuel dependent on the combination to the liquid substances.

Among the three types, BDR and GLDR accompany a decrease in the friction coefficient, C_f, in Eq. (1). In particular, BDR totally depends on how the friction coefficient changes when bubbles are mixed into the boundary layer. We need to learn what happens to the inner layer of the turbulent boundary layer as the friction coefficient changes (Kim 2003). If the friction coefficient increases largely, the

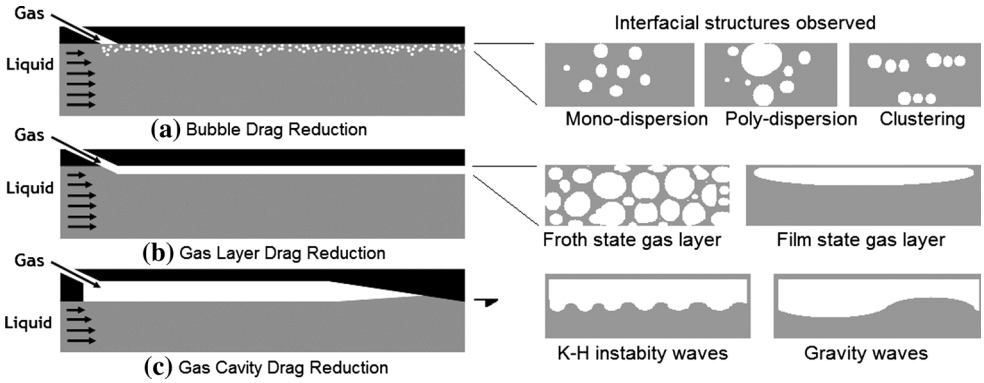

Fig. 1 Three types of frictional drag reduction enabled by gas injection. **a** Bubble drag reduction. **b** Gas layer drag reduction. **c** Gas cavity drag reduction (Mäkiharju et al. 2013a, b)

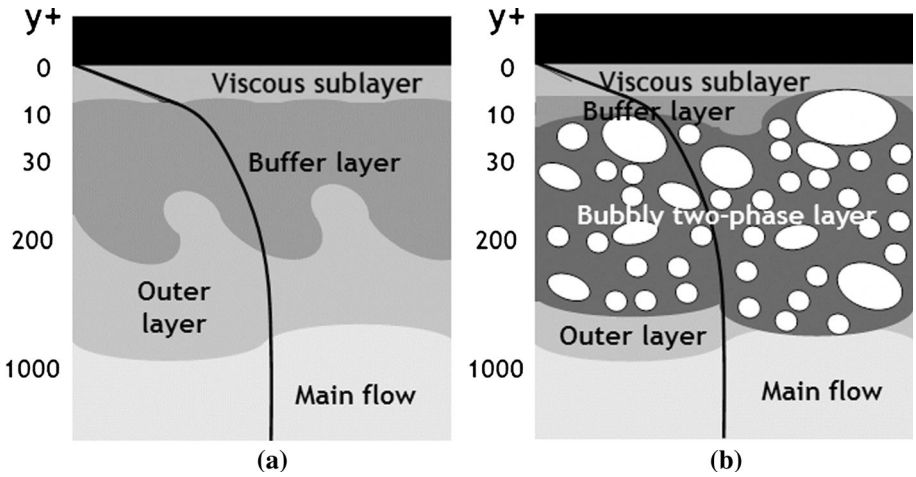

Fig. 2 Question how bubble injection alters the inner structure of a turbulent boundary layer. **a** General view of shear layer decomposition. **b** The question of how bubbles alter the original structure by replacing with a bubbly two-phase layer

decreasing effect of the fluid density or the area of contact would be canceled out. If C_f reduces together with the fluid density and area of contact, drag reduction would be amplified according to their synergy effect. This is the point of focus in this article. The change in friction coefficient owing to the presence of bubbles clearly declares that the inner layer structure differs from that of single-phase flow. Gabillet et al. (2002) found in a horizontal turbulent channel flow with upward bubble injection that the bubbles activated near-wall turbulence that increased linearly with the void fraction. They concluded that the bubbles remaining near the wall affect the boundary layer in a way similar to wall surface roughness, thus increasing drag. Non-spherical bubbles of intermediate size in the wall proximity potentially increase the friction coefficient, which is analogous to the enhancement of heat and mass transfer owing to the presence of such bubbles (Kitagawa et al. 2008). As buoyancy acts on the boundary layer outward, the boundary layer thickness expands so that drag can be reduced (Aliseda and Lasheras 2006). Recent papers reported that dilute mixing of microbubbles comparable to or smaller than turbulent eddy scales can sensitively reduce the friction coefficient (e.g., Hara et al. 2011). For inertial deformable bubbles at high Weber numbers, drag reduction is restored owing to the collapse of coherent structures (Huang et al. 2008). In this context, we should consider the multiple roles played by bubbles in a single case of boundary layer flow. As bubbles of broad size are injected, these roles overlap in the same flow field to be intertwined complicatedly. This issue is addressed below.

Figure 2 schematically shows the influence of bubbles when they are mixed inside a turbulent boundary layer. Initially, there are multiple different shear layers from the wall: a viscous sublayer, buffer layer, outer layer, and main flow region (Robinson 1991; Adrian 2007). The number of layers depends on how precisely we observe the individual role of turbulence (Jimenez 2012). Once bubbles are mixed, such detailed discussion of the single-phase boundary layer raises two major questions. The first question relates to where the bubbles tend to remain. Even in flow without turbulence, bubbles have their own fluctuating nature owing to the time-lagging combination of transversal force components, such as the drag, lift, added inertia, pressure gradient, and history forces. Deformability of bubbles at high shearing turbulence introduces further stochastic behavior. The second question relates to how the bubbles create a new layer that replaces the original layer. Fluid behavior within the new layer obeys the rule of bubbly two-phase flow dynamics, and hence it is not approximated by any single-phase flow models. Evidence is available from pipe and channel flow experiments whose pressure drop characteristics of gas–liquid two-phase flow are indescribable only with the mixture property of two fluids (Lundin and McCready 2009). Well-known interfacial patterns in a tube such as bubbly flow, plug flow, slug flow, froth flow, and stratified flow can occur analogously in the two-phase shear layer sandwiched by the wall and outer region. Historical studies on internal two-phase flows remind us that drag reduction by bubble injection is at the heart of the issue of multiphase flow.

2.2 Mechanism transition diagram

Understanding of the mechanism of transition allows reasonable design of drag reduction and improved performance. Unfortunately, the mechanism in use of bubbles is not explained by a couple of dimensionless parameters. What we see from data available today is a series of correlations among the liquid flow speed, gas flow rate, mean bubble size (often lacking), and drag reduction ratio for a number of different flow configurations. Everything in the bubble–liquid interaction differs between internal and

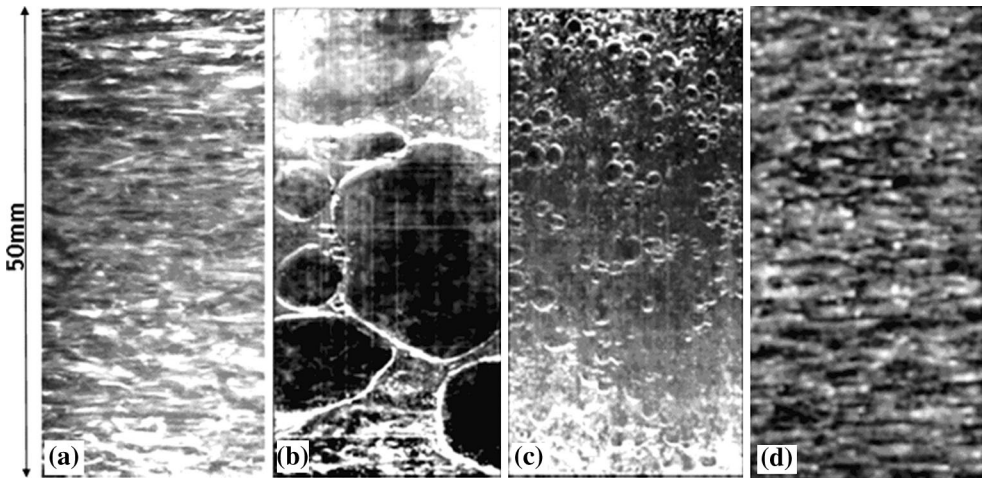

Fig. 3 Kaliroscope visualization of turbulent eddies in a horizontal channel flow at 2 m/s. The main stream flows from left to right. Near-wall eddies are illuminated with a sheet of light in the spanwise direction so that streamwise vortices are mainly visualized. **a** Without bubbles, **b** with large bubbles, **c** with small bubbles, **d** with microbubbles (Murai et al. 2006a, b, c)

external flows, between fully developed and spatially developing flows, and between horizontal and vertical streams. There have been intensive studies to date on the turbulent flow characteristics of bubbly two-phase flow in a cylindrical tube (Lockhart and Martinelli 1949; Fujiwara et al. 2004; Hosokawa and Tomiyama 2004, 2009; Ishii and Hibiki 2011). As the diameter of the tube changes, not only the Reynolds number but also all other dominant dimensionless numbers change simultaneously such as Froude number, Weber number, capillary number, Rayleigh number, and Mach number. Buckingham's Π theorem does not immediately benefit researchers in terms of reducing the number of experimental parameters. Engineers accept dimensional consolidation of the measurement data since the physics is still only half understood. In application to vessels, there are further uncontrollable factors of the boundary layer, which make the causal relationship between the fuel consumption rate and bubbling flow rate unclear (Mizokami et al. 2010; Mäkiharju et al. 2012; Kumagai et al. 2010). The drag reduction performance of vessels is affected by the specifics of each vessel, meteorological factors, and seawater properties. The overlap of fluid dynamic nonlinearity in multiphase turbulent flow and the diversity of ship operation conditions mean that there is a severe lack of reproducibility in ship drag reductions. With such problems in application, engineers emphasize the importance of fundamental study that can classify the phenomenon into known and unknown domains, or into reproducible and irreproducible regions of parameter space.

Figure 3 shows the effect of bubbles on the turbulent flow structure, as observed from the top of a horizontal water channel flow (Murai et al. 2006a, b, c). Bubbles of three different sizes are injected into water that flows at 2 m/s. The stripe pattern in the left photograph (a) indicates turbulent eddies close to the wall, visualized by Kalliroscope [details of which were given by Dominguez-Lerma et al. (1985)]. Photograph (b) is a snapshot of the same flow when large bubbles are injected. The stripe pattern is attenuated inside the area with bubbles, but remains in the area without bubbles. Photograph (c) shows the case of small bubbles, ranging from 1 to 5 mm in diameter. Since the bubble size and the spacing of streamwise vortices are comparable to each other, the original stripe pattern disappears. Photograph (d) is a snapshot when microbubbles of 50 μm in peak diameter are mixed into the channel flow at a volume fraction of 0.01 %. The stripe pattern is revived, but the spatio-temporal frequency changes. The photographs clearly show that the bubble–turbulent flow interaction has different mechanisms according to bubble size.

Before reviewing the individual findings reported in past papers, the experimental conditions that each researcher employed are classified. Figure 4 plots the results of published papers on a two-parameter domain, with the abscissa giving the bubble size and the ordinate giving the flow speed. The plot includes results for horizontal channel flow, flow along horizontal flat plates, and model ships. It excludes results for the drag reduction of vertical pipe flows, vertical channel flows, and Taylor–Couette flows because different flow configurations need another comparison on different plots. Numerical analysis is also excluded. The plot shows that the success of drag reduction is roughly separated into two regions. One is the use of relatively small bubbles at high flow speed (marked in M and S), and the other is the use of large bubbles at low flow speed (marked in L and V). Between these two regions, few papers reported the success of drag reduction as

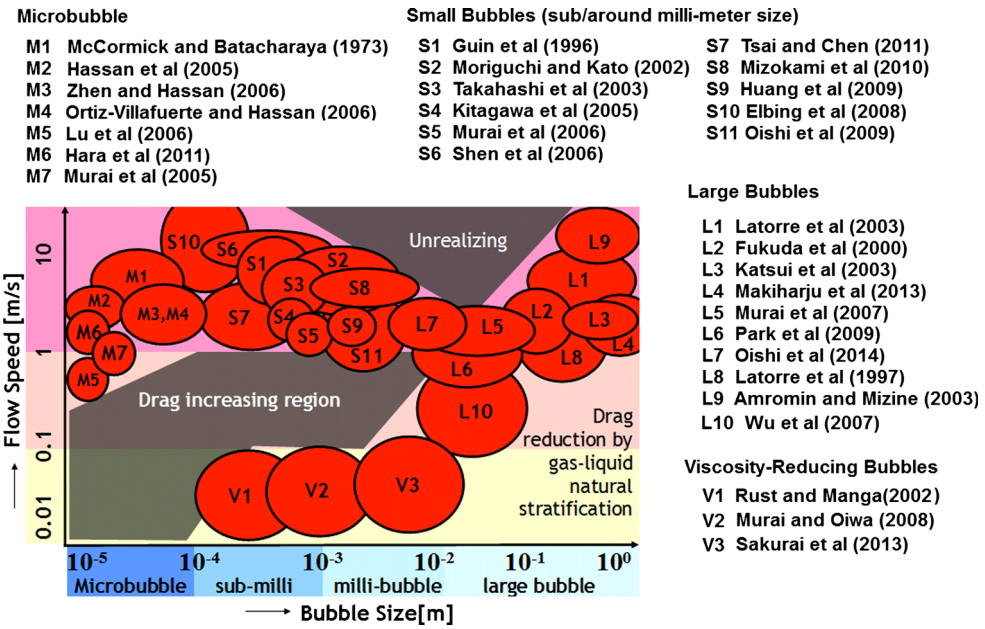

Fig. 4 Distribution of technical papers on the experimental success of drag reduction plotted on a two-parameter domain. The central position and diameter of each ellipse indicate the average conditions and the approximate range of experimental tests in each report

indicated by gray regions. In the gray regions, the injection of bubbles rather increases the friction, whereas the mixture density of the boundary layer is invariably reduced. We have to avoid the condition falling in these regions to guarantee drag reduction. The upper gray region "Unrealizing" means that bubbles become unstable to keep their initial size owing to shear stress. This region takes place only in the transition from small to large bubbles for coalescence at high void fraction or large to small bubbles for fragmentation.

Table 2 lists all available reports on drag reduction using horizontal channel flows. The reports are roughly classified by mean bubble size. Results from DNS are recognized as numerical experiments and included here. In the "Bubble injection into" column, "beneath" refers to bubble injection beneath the top wall of the channel, and "above" refers to bubble injection from the bottom wall of the channel. The column "Drag reduction %" presents the maximum recorded drag reduction percentage, and "Gain factor" is the ratio of the drag reduction per unit void fraction [see Eq. (5)]. It is noted that these results cannot be simply compared because of the very different conditions applied in each assessment. Nevertheless, drag reduction percentages of several tens have been reported.

Table 3 summarizes reports on drag reduction in other types of flow configurations. The use of a flat plate deals with the bubble effect in a spatially developing boundary layer, different from a fully developed channel flow. In contrast, Taylor–Couette flow is preferably adopted to assess the fully developed state of two-way interaction between bubbles and turbulence. Application to ships or model ships also recorded drag reduction in some cases; however, it should be noted that failures in drag reduction of ships were rarely published in journal articles. The author is aware of a number of failures in ship drag reduction via collaborations and private communications. Accordingly, exact experimentations for fundamental flow configurations are strongly desired. In the following subsection, the performance and mechanism of drag reduction in each region are elaborated.

2.3 Gas cavity effect regime

Frictional resistance is reduced by having a gas cavity between a solid wall and outer flow. Fukuda et al. (2000) demonstrated that this effect is in proportion to the ratio of the area covered by gas to the whole area of the wall. The mechanism is explained simply: The gas cavity cuts off the contact between the liquid flow and the wall. However, maintaining a stable gas cavity close to the wall requires technical efforts. In case of external flow around a high-speed moving body, blowing air from the front demands a gas flow rate larger than a critical value to keep the gas–liquid interface at the desired position. Cavitation-relevant phenomena are coupled with the technique, implicitly or explicitly (Callenaere et al. 2001). For slow flows below a flat wall, the gas cavity naturally forms with buoyancy and can stably remain beneath the wall. In both cases, an increase in flow speed results in a wavy gas–liquid interface owing to Kelvin–Helmholtz instability (Michel 1984). In particular, the combination of high-speed liquid flow and slow gas flow amplifies the instability so that the gas cavity is easily broken into an ensemble of bubbles as it migrates a long way downstream. Amromin and Mizine (2003) analyzed possibility of active flow control to keep partial cavity stable. Even in the case of a gas cavity subject to

Table 2 Reports on drag reduction for bubble injection into horizontal channel flows

Flow configuration	Bubble size	Year	Investigators	Bubble injection into	Drag reduction %	Gain factor	Central bubble size
Horizontal channel flow	Large bubbles	1963	Hirata and Nishiwaki	Beneath	15	0.5	100 mm
		2002	Gabillet, Colinm, and Fabre	Above	<0	<0	10 mm
		2007	Murai, Fukuda, Oishi and Kodama	Beneath	60	2	>10 mm
		2009	Park, Tasaka, Murai, and Oishi	Beneath	25	20	>40 mm
	Small bubbles	1985	Madavan, Deusch, and Merkle	Above	80	1.5	Broad
		1995	Kim and Clever	Beneath	65	NA	NA
		1996	Guin, Kato et al.	Beneath	20	2	0.5 mm
		1999	Kato, Iwashina et al.	Beneath	60	4	0.5 mm
		2000	Kodama, Kakugawa et al.	Beneath	30	3.5	NA
		2002	Moriguchi and Kato	Beneath	40	4	0.5–2.5 mm
		2005	Kitagawa, Hishida, and Kodama	Beneath	2.5	5	0.5 mm
		2006	Shen, Ceccio, and Perlin	Beneath	35	3.5	0.05–0.4 mm
		2006	Murai, Oishi, Takeda, Yamamoto	Beneath	10	1.5	0.5 mm
		2009	Huang, Murai, Yamamoto	Beneath	5	2	1 mm
		2009	Oishi, Murai, Tasaka, Takeda	Beneath	10	4	1 mm
	Microbubbles	2005	Hassan, Gutierrez Torres et al.	Beneath	38	10	0.05 mm
		2005	Murai, Oishi, Sasaki, and Kodama	Beneath	20	1,000	0.03 mm
		2005	Lu, Hamada, and Kato	Beneath	25	800	0.03 mm
		2011	Hara, Suzuki, and Yamamoto	Beneath	20	1,100	0.03 mm
	DNS	2002	Xu and Maxey	Spherical	15	1.5	Spherical
		2002	Kawamura and Kodama	Deformable	<0	−3	$We = 37$
		2005	Lu, Fernandez, Tryggvason	Deformable	25	1.3	$We = 0.4$

slow flows, a gravity wave forms as another factor of interfacial instability as analyzed by Matveev (2007). Once the wave touches the wall, the cavity transforms to dynamic two-phase flow similar to froth and churn flow. The main parameter that governs the gas cavity regime is the Froude number defined by

$$Fr = \frac{U}{\sqrt{gL}}, \tag{2}$$

where U, g, and L are the characteristic flow speed, acceleration of gravity, and characteristic length of the flow configuration. When Fr is sufficiently smaller than unity, the buoyancy force stabilizes the gas cavity. For $Fr > 1$, waves are generated downstream to destroy the cavity. The following investigation on such application of an gas cavity has been reported.

Katsui et al. (2003) measured the drag reduction ratio of a model ship in the cavity regime. They employed partitions on the bottom of the ship to provide 12 independent air cavities so that a certain tolerance to waves and ship oscillation was secured for $0.1 < Fr < 0.2$. In terms of power savings, the gas flow rate required for generating and maintaining the air cavity needs to be minimized. This raises two questions: How the gas cavity works properly for drag reduction as its thickness decreases, and how the gas cavity maintains its function as its length in the main flow direction is shortened. In flow geometry of backward facing step, Mäkiharju et al. (2013a, b) found dependences of air cavity formation on Reynolds and Weber numbers which correlate with gas shedding from the cavity. At enough high Reynolds numbers, their dependences are relaxed and high drag reduction ratio up to 95 % was confirmed within the cavity closure (Lay et al. 2010). Their work supports design of necessary ventilation flow rate to maintain the gas cavity drag reduction. Amromin et al. (2011) designed a ship hull with a bottom niche terminating in a cavity locker, which suppresses cavity tail oscillations and reduces the escape of gas from the cavity. They obtained approximately 25 % drag reduction for $0.4 < Fr < 0.7$ in a seaway and the power required to supply gas was less than 4 % of the gain in the required propulsion power.

2.4 Gas layer effect regime

In ordinary applications, gas cavity is provided artificially such as by a stern (see Fig. 1c). When the name of gas cavity changes to gas layer, it indicates that gas phase thickness is minimized necessary for isolating liquid from

Table 3 Reports on drag reduction for bubble injection into various configurations of shear flows

Flow configuration	Flow configuration	Year	Investigators	Bubble injection into	Drag reduction %	Gain factor	Central bubble size
Flat plate boundary layer		2004	Ferrante and Elghobashi	DNS	20	10	0.06 mm
		2006	Sanders, Winkel, Dowlingm et al.	Beneath	90	3	0.3 mm
		2007	Wu, Hsu, Lin	Beneath	25	5	Broad
		2008	Elbing, Winkel, Lay, and Ceccio	Above	25 to 80	2 to 4	Broad
		2010	Jacob, Olivieri, Miozzi et al.	Beneath	9	250	0.15 mm
		2013	Elbing, Makiharju, Wiggins et al.	Above	95	1.5	Air layer
		2013	Mäkiharju, Perlin, and Ceccio	Beneath	90	1	Air Cavity
Taylor–Couette flow		2002	Rust and Manga	Laminar	50	1.7	1 mm
		2007	van den Berg, Luther et al.	Turbulent	25	3	1 mm
		2008	Murai, Oiwa, Takeda	Turbulent	35	7	0.5 mm
		2008	Sugiyama, Calzavarini, Lohse	CFD	20	20	0.5 mm
		2013	van Gils, Guzman, Sun, Lohse	Turbulent	40	13	1 mm
		2013	Watamura, Tasaka, Murai	Transition	20	800	0.06 mm
		2014	Maryami, Farahat et al.	Turbulent	11	3	1 mm
Ship and model ship		1973	McCormick and Bhattacharyya	Submerged	20	200	Microbubbles
		1997	Latorre	Ship	30	1	Air cavity
		2000	Fukuda, Tokunaga et al.	Model ship	20	1	Air cavity
		2003	Latorre, Miller, and Philips	Model ship	11	0.2	Small bubbles
		2003	Takahashi, Kakugawa et al.	Model ship	40	1	Small bubbles
		2003	Katsui, Okamoto et al.	Model ship	80	1	Air cavity
		2010	Foeth, Eggers, and Quadvlieg	Ship	Total 0	0	NA
		2010	Mizokami, Kawakita, Kodan et al.	Ship	Total 12 %	NA	NA
		2011	Amromin, Karafiath, and Metcalf	Ship	Local 25 %	NA	Air cavity
		2012	Mäkiharju, Perlin, and Ceccio	Ship	Total 14 %	NA	Air cavity
		2010	Kumagai, Murai, and Takahashi	Ship	Total 14 %	NA	Small bubbles
Others							
Pipe flow		1997	Liu	Laminar	<0	−6	2 mm
		2005	Serizawa, Inui, and Eguchi	Transition	75	150	0.04 mm
Sphere		2003	Cui, Fan, and Park	Turbulent	15	NA	0.01 mm
		2008	Murai and Oiwa	Laminar	−10	−3	2 mm
Spin shear		2013	Sakurai, Tasaka, and Murai	Laminar	−60	−30	2 mm

Gain factor is defined by drag reduction ratio divided by bulk void fraction which depends on flow geometry

Data in company's website and unauthorized publications are excluded

the wall. Hence, gas layer is called so when the gas-occupying thickness is less than the boundary layer thickness. On this condition, we see two-phase flow patterns such as film flow, froth flow, and horizontally elongated flat-bubble flow.

The wall coating of a hull for stabilizing a gas cavity was examined by Fukuda et al. (2000). They applied a super water-repellent coating and achieved 80 % drag reduction at flow speeds from 4 to 8 m/s. Their result implied that total replacement of water with gas is unnecessary in the boundary layer as long as a thin gas film remains on the wall surface. The concept of introducing a super hydrophobic surface into the wall boundary layer was proposed by Lee and Kim (2011). Once the wall structure is allowed to change, stationary arrangement of bubbles in a desired pattern can support the drag reduction as reported by Kwon et al. (2014).

Elbing et al. (2013) investigated how much gas flow rate is required to keep the gas layer drag reduction, not falling into bubble drag reduction. They found its critical value based on scaling for experimental data considering the lift and buoyancy of dispersed bubbles. Their gas layer contained void fraction of 75 % within the boundary layer thickness.

The relationship between the length of the gas bubble elongated in the main stream direction and local skin friction was measured by the author's group (Murai et al.

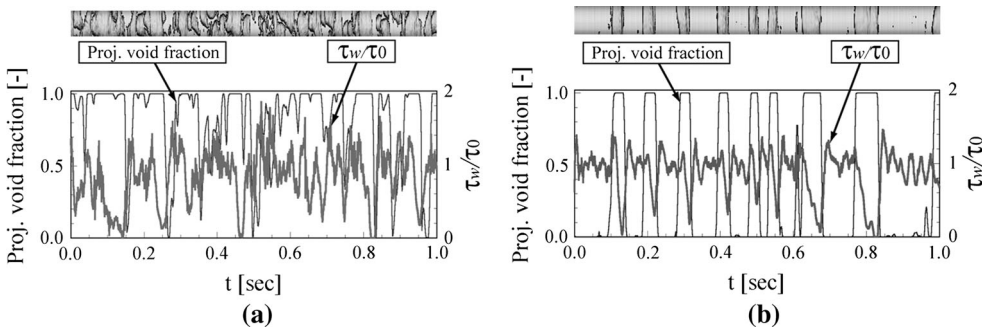

Fig. 5 Temporal fluctuation of the local wall shear stress owing to the passage of large bubbles in a horizontal air–water turbulent channel flow having a bulk mean liquid velocity of 1.0 m/s and bulk mean void fraction of 20 %. The projected void fraction is defined by the ratio of the area occupied by the bubble image on the wall within the circular area of the wall shear stress sensor (Murai et al. 2007)

2005a, b). Figure 5 shows two samples of the results obtained by synchronized measurement of the local wall shear stress and local void fraction on the wall inside a horizontal channel flow. They found that bubbles longer than about five times the boundary layer thickness reduce the average drag around them. This tells that drag reduction by gas cavity approach requires this length scale at least in each unit. In contrast, shorter bubbles are not as effective in reducing drag. Characteristics of such drag-neutral and drag-increasing bubbles will be elaborated in the final part of this chapter.

While the gas cavity technique has not been linked to turbulence modification, it obviously alters the local turbulence close to the gas–liquid interface. Velocity fluctuations in the tangential direction of the interface are conserved, but those in the normal direction are restricted so that turbulence travels in two dimensions (Ouellette 2012). Hence, the scenario of drag reduction employing the gas cavity technique involves curious scientific phenomena such as the inverse cascade of two-dimensional turbulence (e.g., Boffetta et al. 2000). As long as the coherent structure of turbulence is smaller than the length scale of the gas–liquid interface, long bubbles also provide local two-dimensionalization of turbulence around them as recently visualized quantitatively by Oishi and Murai (2014) and Park et al. (2014).

2.5 Microbubble regime: bubbles smaller than coherent structures

As small bubbles are mixed into liquid, they interact with turbulence and the original turbulent structure inside the boundary layer is modified. The Reynolds number expresses the target flow field attacked by small bubbles;

$$Re = \frac{UL}{\nu}, \tag{3}$$

where U, L and, ν are the characteristic flow speed, characteristic length of the flow configuration, and kinematic viscosity of the liquid. Since turbulence has a broad spectrum in terms of wavelength and frequency, bubble–turbulence interaction is deduced according to the bubble size. While there are still deep discussions on the scaling problem, the influence is classified at least into two cases. One is the case that bubbles are smaller than tens of the wall unit of the boundary layer. Another is the use of bubbles larger than those in the first case, but smaller than the boundary layer thickness. The wall unit, l^+, is defined by

$$l^+ = \frac{\nu}{u_\tau}, \quad u_\tau = \sqrt{\frac{\tau_w}{\rho}}, \quad \tau_\mathrm{w} = C_\mathrm{f}\frac{1}{2}\rho U^2, \rightarrow l^+ = \frac{\nu}{U}\sqrt{\frac{2}{C_\mathrm{f}}}, \tag{4}$$

where u_τ and ρ are the friction velocity and density of the liquid. τ_w and C_f are the wall shear stress and friction coefficient. For an air–water combination with flow speed of several meters per second, the wall unit becomes roughly 10 μm. Hence, bubbles larger than 100 μm will directly attack the coherent structures in turbulence with their volume effect. In contrast, bubbles smaller than 100 μm alter the internal fluid properties inside individual eddies. In both cases, the coherent structures that are a source of friction can be modified in the following mechanism.

The effects of small particles and microbubbles on the turbulent boundary layer are commonly explained up to a point. Small solid particles tend to stay in low-speed streak regions (Narayanan and Lakehal 2003), and they alter the coherent structure around them so that drag is reduced (Zhao et al. 2010, 2012). Such turbulent structure modified by solid particles was summarized by Gore and Crowe (1989, 1991) and Crowe et al. (1996). They clarified that particles smaller than 1/10 of integral length scale of turbulence always relax the turbulent intensity. Motion of solid particles in turbulence was reviewed by Toschi and Bodenschartz (2009). The main difference of microbubbles from solid particles is their own density relative to that of

the continuous phase, which provides opposite Lagrangian acceleration relative to that of the continuous phase as the same pressure gradient acts on them. A number of numerical research works have investigated this topic prior to experimental demonstrations. Felton and Loth (2001, 2002) simulated the wall-perpendicular diffusion process of small spherical bubbles during downstream migration. The diffusion of bubbles is caused by a random diffusion in turbulence, and it is thus promoted with a spatial gradient of turbulence intensity that decreases with distance from the wall. The phenomenon is the same as that observed for solid particles and dye as can be simulated by Reynolds average model equations. Xu et al. (2002) simulated the drag reduction performance provided by spherical bubbles in a DNS for a turbulent channel flow. They simulated bubble–liquid interaction at a nominal channel Reynolds number of 3,000 and bubble diameters of several tens of wall units. They found the realization of significant drag reduction in the transient process of bubble diffusion, which ceased as the void fraction reached a steady profile. Ferrante and Elghobashi (2004, 2005) carried out a DNS for a spatially developing turbulent boundary layer at a Reynolds number of 1,400–3,000. Their interpretation of the result is that the motion of small bubbles provides positive divergence of the liquid velocity vector field close to the wall, and the bubbles push the streamwise vortical structures away from the wall.

It should be noted that in the field of numerical simulation, the term "microbubbles" is used when bubbles are treated as spheres. Upon the spherical assumption, the mathematical description of two-phase flow is dramatically simplified as described by the Eulerian–Lagrangian formulation and point-source approximation based on Stokesian dynamics. Consequently, the computational load of the DNS is lightened, and therefore, numerical research on microbubble drag reduction has progressed more quickly than research on drag reduction by non-microbubbles. Experimentalists use the term "microbubbles" for a bubble size that is actually several tens of microns. In clean water, the lower size limit of non-condensable microbubbles that survive against their own surface tension is around 5 μm (e.g., Fujikawa et al. 2011). The upper limit may be submillimeter size, at which bubbles start to show non-spherical deformation in turbulence. The first experiment on microbubble drag reduction by McCormick and Bhattacharyya (1973) employed water electrolysis. The mean bubble diameter estimated using their setup is probably tens of microns although they did not clearly state this. Microbubble generation with water electrolysis did not come up in the literature again until 2003. Engineers believed for 30 years that there was no significant difference between submillimeter bubbles and microbubbles.

The first experiment performed this century on microbubbles was that carried out by Hassan and Ortiz-Villafuerte (2003). They presented significant drag reduction performance for a horizontal channel flow when hydrogen microbubbles were mixed with water electrolysis. In their later papers (Hassan et al. 2005; Zhen and Hassan 2006; Ortiz-Villafuerte and Hassan 2006), they reported that the action of microbubbles destroys coherent structures. The author's group also examined the effect of hydrogen microbubbles in a 2-m/s channel flow (Murai et al. 2005a). They obtained 20 % drag reduction with only a 0.02 % bubble volume fraction. The sensitivity of the drag reduction per unit void fraction can be evaluated by

$$G \equiv \frac{\Delta D/D}{\alpha} = \frac{1}{\alpha}\left\{1 - \frac{C_{\mathrm{f}}}{C_{f0}}(1-\alpha)\right\}, \tag{5}$$

where D, ΔD, and α are the original drag without bubbles, reduced drag as bubbles are injected, and void fraction, respectively. The right-hand side is the formula when Eq. (1) is substituted into the definition. We refer to G as the gain factor of drag reduction; it indicates the amplification of drag reduction relative to the inertia-originating effect of drag reduction. When the friction coefficient is unmodified by bubbles, G becomes unity. Most gas cavity methods have a value of G around unity.

In the author's first experiments on microbubbles, the value G was obtained surprisingly to be 1,000 at $Re = 10^4$ (Murai et al. 2005a). In the experimental facility, water electrolysis apparatus for generating both hydrogen and oxygen microbubbles was flash mounted on the top surface of the channel so as not to affect on the liquid boundary layer downstream. The results of a succeeding experiment using the same facility was reported later by Hara et al. (2011) after careful checking of reproducibility in terms of the performance of bubble generation around the electrodes. Figure 6 shows their experimental data, confirming that the impact of the microbubble was on the same order; $G = 1{,}100$. According to their PTV measurement, Reynolds shear stress was reduced effectively only in the vicinity of the wall and that in the downstream region soon recovered and rather increased outside the original boundary layer. They attributed the dramatic drag reduction to the transient process of microbubble motion along the main stream. Lu et al. (2005b) constructed a clone of Hara's bubble generation device for their different horizontal channel facility and obtained nearly the same degree of drag reduction; $G = 800$. For water flows beneath a horizontal flat plate, a large effect of microbubbles of $G = 250$ was measured by Jacob et al. (2010). They found by their PIV a decrease in coherency of the near-wall structure. For different flow geometry, large gain factors were obtained by Serizawa et al. (2005) for microbubble pipe flows (around $G = 150$) and by Watamura et al. (2013) for microbubble-added circular Couette flows ($G = 800$).

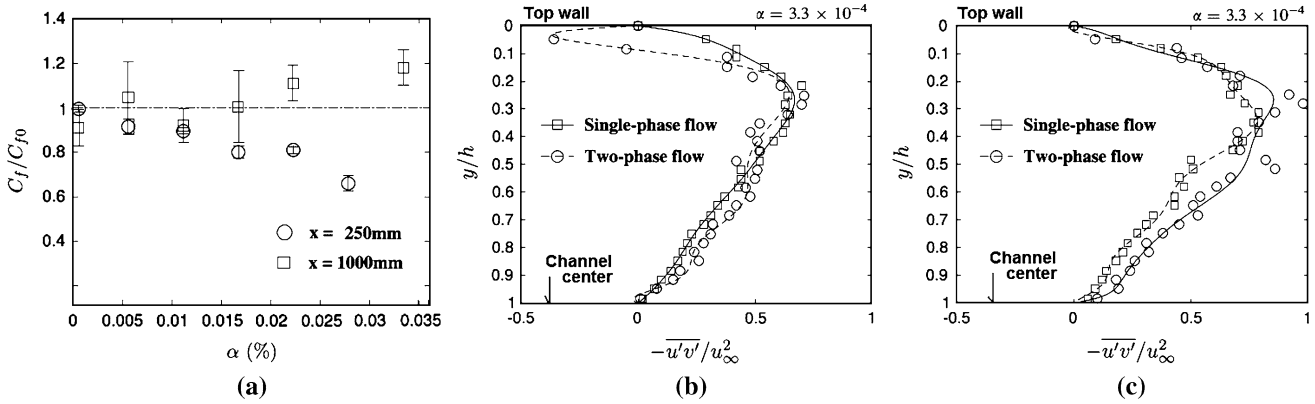

Fig. 6 Sensitive drag reduction resulting from microbubbles observed in a finite region from the bubble injection point. **a** Friction coefficient relative to the single phase. **b** Reynolds shear stress profiles measured by PTV at 250 mm from the bubble injection point. **c** The same profiles at 1,000 mm from the injection point (Hara et al. 2011)

All the above experimental results are explained by the action of spherical bubbles on the coherent structure in turbulence. As shown by numerical analysis of Maxey et al. (1996), microbubbles concentrate into strong vorticity regions, but low strain rate in Stokes regime of microbubble motion. L'vov et al. (2005) stated that the volumetric effect of microbubbles is lost as the microbubble diameter decreases. Their linearized theory inferred that drag reduction remains as observed in the single-phase turbulent boundary layer that has wall-perpendicular distributions of density and viscosity if clustering of microbubbles is ignored. However, the mechanism in the microbubble regime is hardly unified as a single mathematical model, consequently. Particularly for gain factors obtained on the order of hundreds, another scenario must be introduced, which will be picked up at the end of Sect. 2.8.

2.6 Mesoscopic bubble regime: bubbles comparable in size to coherent structures

The most difficult case for understanding the drag reduction mechanism may be that when the bubble size is comparable to the length scale of coherent structures. This is so in both experimental and numerical studies. This condition is, however, the most frequently appearing in laboratory experiments and practical application because such bubbles are easily and naturally realized in the air–water combination of bubbly flow. This is explained with a Weber number defined by

$$We = \frac{\rho U_{\mathrm{d}}^2 d}{\sigma}, \quad U_{\mathrm{d}} = \left|\frac{\mathrm{d}u}{\mathrm{d}y}\right| d, \tag{6}$$

where U_{d} is the differential velocity of the liquid phase between two points on a single bubble surface, d is the bubble diameter, and σ is the surface tension of the bubble interface. Bubbles that have a Weber number larger than the critical Weber number (which is around 10) are unstable and fragment into multiple small bubbles and such large bubbles thus disappear downstream. The diameter of the largest bubble that survives in turbulent shear flow is estimated by substituting the local shear rate into Eq. (6):

$$d^3 = \frac{\sigma}{\rho}\left|\frac{\mathrm{d}u}{\mathrm{d}y}\right|^{-2} We_{\mathrm{c}} \leftarrow \tau_{\mathrm{w}} = \mu\left|\frac{\mathrm{d}u}{\mathrm{d}y}\right| = C_{\mathrm{f}}\frac{1}{2}\rho U^2. \tag{7}$$

Hence, the upper limit of the bubble diameter is obtained as

$$d = \left\{\frac{4\sigma}{\rho}\left(\frac{\nu}{C_{\mathrm{f}}U^2}\right)^2 \mathrm{We}_{\mathrm{c}}\right\}^{1/3}. \tag{8}$$

The above formula infers that the largest bubble in a 5-m/s air–water bubbly two-phase boundary layer has a diameter of 500 μm, which is comparable with the length scales of coherent structures such as the spanwise spacing of streamwise vortices, sweeping flow into the wall, and bursting eddies. In the region far from the wall, the local shear rate is lower and the upper limit of the diameter thus higher. Equation (8) also indicates that the upper limit of the diameter is a function of flow speed, U, to the power of −4/3. This fragmentation theory furthermore reminds us that a histogram of the bubble size will have a peak population close to the upper limit of the diameter at each position from the wall. The bubbles having diameters around the upper limit always behave non-spherically and deform unsteadily in turbulence. Consequently, the mechanism of drag reduction in this regime requires insights not only into the volume-comparable effect with coherent structures but also into the role of bubble deformation in turbulence. This issue outweighs the density effect in maintaining steady drag reduction as explained later in Sect. 3.1. Consequently, bubble breakup and bubble deformation should be always considered in a couple.

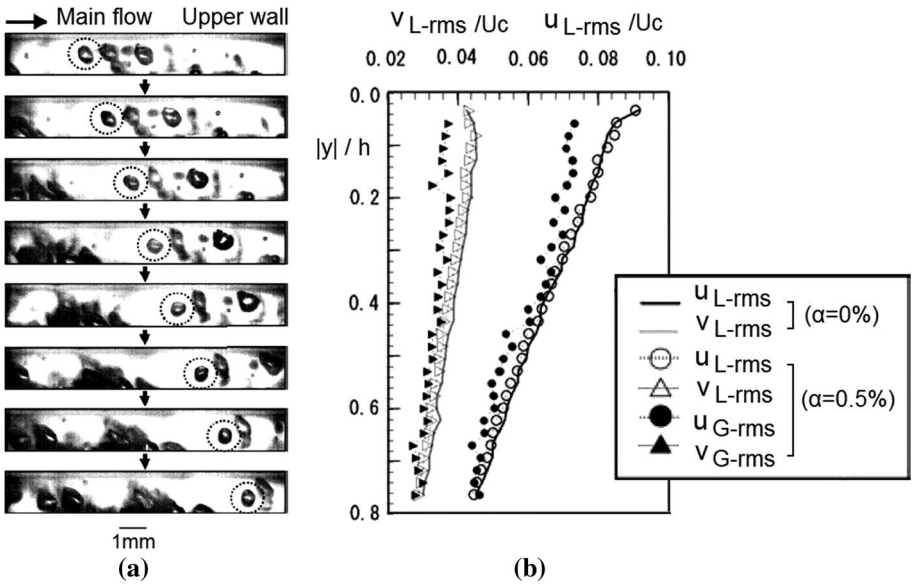

Fig. 7 Complex unsteady bubble deformation in the wall proximity of a horizontal channel flow. **a** Eight consecutive images taken over a period of 2 ms. **b** Profiles of the root mean square of the velocity fluctuation in both phases, indicating that the translational velocity fluctuation of the bubbles is relaxed significantly by the deformability of bubbles in strong turbulence (Kitagawa et al. 2005)

Equation (8) just estimates it in semiempirical form at dilute bubble situations. There are papers published on shear-triggered bubble breakup phenomena such as Hinze (1955), and Hesketh et al. (1991).

Kato et al. (1999) and Moriguchi and Kato (2002) performed horizontal channel flow experiments and found that the dependency on bubble size was insignificant in their tested range. Towing test experiments for a flat plate conducted by Takahashi et al. (2003) and for a catamaran conducted by Latorre et al. (2003) showed stable drag reduction that was linear to the gas volume flow rate, whereas the bubble size was not so carefully controlled. Shen et al. (2006) used surfactant to examine the effect of the mean bubble size in a turbulent channel and concluded that their drag reduction was insignificantly affected by the bubble size. The gain factors in these experiments ranged from 1.5 to 3.5; i.e., they were larger than unity.

To mechanism-pursuing researchers, the bubble size insensitivity appears to be rather curious. Kitagawa et al. (2005) found a reason for the insensitivity. Their particle tracking velocimetry for two-phase flow at 5 m/s and a mean bubble diameter of 500 μm revealed that a bubble's soft deformation owing to surrounding turbulence absorbs Reynolds shear stress as shown in Fig. 7. The concept was already known to Serizawa and Kataoka (1990), who modeled bubble deformability in isotropic turbulence as a temporal absorber of kinetic energy that then released the kinetic energy with a time lag. The time lag is on the order of the resonance period of oscillation of the bubble shape (Ryskin and Leal 1984). For the air–water combination, the resonance period of the upper limit of the diameter is much longer than the timescales of coherent structures so that bubble deformability dampens the local acceleration of turbulence. This explains why deformable bubbles, no matter the precise control of bubble size, work robustly for drag reduction.

DNS of the mechanism of the interaction between turbulence and deformable bubbles or droplets in turbulent shear flow was reported in several papers. Iwasaki et al. (2001) found that droplets in turbulent Couette flow attenuated a near-wall streamwise vortex with their deformability. Kawamura and Kodama (2002) analyzed a similar flow field for air bubbles and found that bubble deformation altered turbulence statistics. In their simulation, there was an increase in drag owing to the DNS-performable limit of the Weber number. That is, the volume effect that enhances momentum transfer was stronger than the deformability effects. Iwasaki et al. (2001) confirmed the same tradeoff phenomenon between the volume effect and deformability effect of immiscible droplets dispersed in a turbulent channel flow. Furthermore, Lu et al. (2005a) numerically confirmed in DNS that the deformability of bubbles leads to a significant drag reduction owing to suppression of streamwise vorticity existing close to the wall, while bubbles that are less deformed provide an additional shear rate near the viscous sublayer to increase drag. The importance of the deformability is re-elaborated later in Sect. 3.1.

2.7 Large bubble regime: bubbles larger than coherent structures

Drag reduction is still provided by bubbles that are larger than coherent structures in the wall proximity, but sufficiently smaller than the boundary layer thickness. The largeness of the bubbles results in high slip velocities

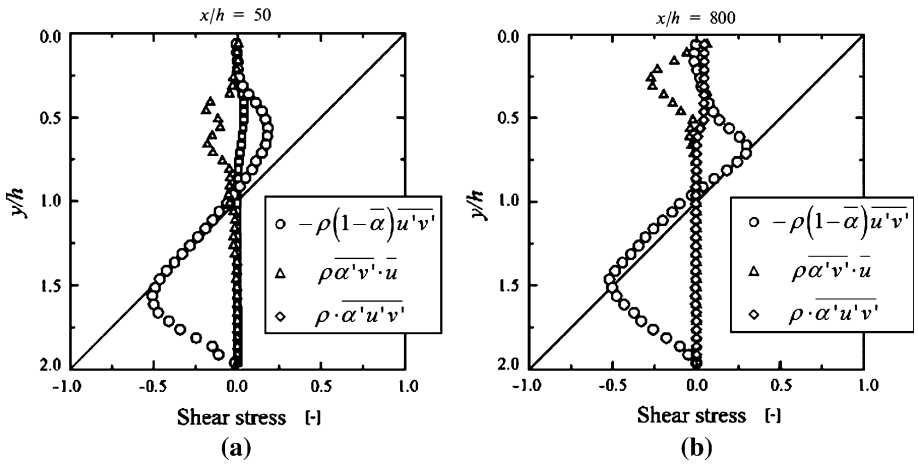

Fig. 8 Profiles of turbulent shear stress decomposed into three terms measured in a horizontal turbulent channel flow. The bulk mean liquid velocity is 2 m/s, and the mean bubble diameter is 0.7 mm relative to the channel height of 2 $h = 10$ mm. **a** Measured profiles at 250 mm (i.e., $x/h = 50$) from the bubble injection point. **b** Measured profiles at 4 m or $x/h = 800$ (Murai et al. 2006b)

between the two phases. The slip velocity is governed in a complex manner, being affected by a combination of seven force components, namely drag, lift, buoyancy, pressure gradient, added inertia, and history forces. These forces act in different directions with time lags among them in turbulence. For such a range of bubble size, Guin et al. (1996) obtained 20 % drag reduction with a bulk mean void fraction of 10 % in a horizontal turbulent channel flow. They found dissimilarity of the void fraction profile in the wall-perpendicular direction as liquid and gas flow rates changed. This implies that drag reduction in this regime should be characterized by spatially developing bubbly flow in the turbulent boundary layer.

Inside the boundary layer, bubbles in this regime repetitively bounce along a wall. The case for a vertical flat wall was investigated by Tran-Cong et al. (2008). The author's group (Murai et al. 2006a) focused on such behavior in a horizontal channel flow. Using bubbles with mean diameter of 0.7 mm in flow traveling at 2 m/s, we observed active oscillation of the bubbles in the wall-perpendicular direction during their migration downstream. The oscillation is attributed to the combination of four dominant forces, namely drag, added inertia, lift, and buoyancy, and could be simulated numerically only with the time-averaged liquid velocity profile. In particular, bubbles close to the wall are rapidly decelerated by the increase in the drag coefficient (Masliyah et al. 1994) and a strong lift force acts on them in the next moment to separate them from the wall again. PTV of both phases by Murai et al. (2006b) revealed that such a cyclic motion of bubbles within the turbulent boundary layer reduced local turbulent shear stress. The mechanism was confirmed by substituting PTV data of the liquid flow field into an equation derived by Reynolds averaging the volume-averaged conservation equation of bubbly two-phase flow:

$$\tau = \mu \frac{\mathrm{d}\overline{u}}{\mathrm{d}y} - \rho(1-\overline{\alpha})\overline{u'v'} + \rho\overline{\alpha'v'}\cdot\overline{u} + \rho\cdot\overline{\alpha'u'v'}, \qquad (9)$$

where α denotes the local void fraction and μ, ρ, u, and v are the viscosity, density, wall-parallel velocity and wall-perpendicular velocity of the liquid phase, respectively. The upper bars and primes, respectively, indicate the time average and fluctuation. These profiles measured at two locations are shown in Fig. 8. The first term is the viscous shear stress, which plays a dominant role in the viscous sublayer, but is negligible outside the layer. The second term is the Reynolds turbulent shear stress, which is relaxed by the average void fraction. This term implies that drag reduction is simply proportional to the void fraction supplied in the boundary layer. This inertia effect of drag reduction in turbulence has been widely confirmed and has a gain factor around unity (Tsai and Chen 2011). However, the correlation of $u'v'$ in the same term can also be modified by the bubbles as the turbulence property changes with them. Thus, the effect of the average void fraction can be amplified. The third term is the shear stress induced by the correlation of $\alpha'v'$, and it is intensified by the mean streamwise velocity. If the flow is perfectively homogeneous without slip between the two phases, this term disappears. The term takes a negative value, contributing to drag reduction, when bubbles have wall-perpendicular oscillations interacting with vortical structures. A simplified interpretation of the term is that such bubbles work as "virtual bursts" instead of liquid turbulence, replacing the sweep and ejection events of the liquid phase with massless bubbles. The opposite effect is known in the case of a heavy particle mixture in boundary layers (Kulick et al. 1994; Taniere et al. 1997). The data of Murai et al. (2006b) show that this term has streamwise persistency as long as bubbles have wall-perpendicular oscillation, and such a phenomenon stands out in the case of relatively large bubbles. How the local turbulence modification in the buffer layer reflects on the wall skin friction was theoretically deduced by Fukagata et al. (2002).

2.8 Rheological effect regime

Even without a slip between bubbles and liquid, the shear stress is still affected by the presence of bubbles. As revealed in the earliest studies of Einstein (1906) and Batchelor (1967), the effective viscosity of a dilute suspension is described by

$$\frac{\mu^*}{\mu_0} = 1 + \frac{\mu_0 + \frac{5}{2}\mu'}{\mu_0 + \mu'}\alpha, \tag{10}$$

where μ^*, μ_0, μ' and α are the effective viscosity, original viscosity of the continuous phase, viscosity within the dispersion phase, and volume fraction of the dispersion. The formula is applicable to dilute spherical dispersion ($\alpha < 0.10$) in simple shear flow. For solid particles, there is no chance to reduce effective viscosity because of $\mu' > \mu_0$. Increasing of the volume fraction exponentially amplifies the viscosity (Stickel and Powell 2005). In the case of a bubbly liquid, the viscosity of gas inside bubbles is sufficiently small compared with that of the liquid and thus

$$\mu^* = (1 + \alpha)\mu_0. \tag{11}$$

Hence, the effective viscosity of the spherical bubble mixture increases. Legner (1984) explained in a qualitative sense that the increase in effective viscosity thickens the viscous sublayer and thus reduces the shear rate. However, the role of the effective viscosity in the entire turbulent boundary layer is still unsolved. Sangani et al. (1997) analyzed the rheological resistance of densely arranged spherical bubbles subject to a rapidly applied shear. They obtained an extra increase in the resistance over that given by Eq. (11) owing to local bubble–bubble interaction. L'vov et al. (2005) coupled the effective viscosity of spherical bubbly liquid with Reynolds-averaged equations and estimated how drag reduction is preserved in homogeneous bubbly flow situations when the void fraction has a wall-perpendicular profile.

The effective viscosity becomes a function of the capillary number as the bubble deforms significantly owing to an increase in the shear rate. Frankel and Acrivos (1970) derived the formula

$$\frac{\mu^*}{\mu_0} = 1 + \frac{1 - \frac{12}{5}Ca^2}{1 + \left(\frac{6}{5}Ca\right)^2}\alpha, \quad Ca = \frac{\mu_0 \gamma}{\sigma}\frac{d}{2}, \quad \gamma = \left|\frac{\mathrm{d}u}{\mathrm{d}y}\right|, \tag{12}$$

which is the same as that derived by Schowalter et al. (1968) when the void fraction is low and where σ, γ, Ca, and d are the surface tension of the bubble surface, shear rate of the liquid around the bubbles, capillary number, and sphere-equivalent bubble diameter. In this formula, the relative viscosity returns to unity at $Ca^2 = 5/12$; i.e., the critical value of Ca at which the sign of the effect on the void fraction changes is $Ca_c = 0.65$. The effective viscosity decreases to values lower than the original liquid viscosity at higher values of Ca. Rust and Manga (2002a) obtained the relationship between Ca and the bubble deformation ratio in simple shear flow and confirmed the validity of the above formula by means of circular Couette flow viscometry (Rust and Manga 2002b). In a typical case of drag reduction for a ship, Ca takes values that cross the critical capillary number as the local shear rate is defined by the coherent structures in the boundary layer. It is thus deduced that the shear-thinning property of the bubbly liquid affects turbulence. Zhen et al. (2013) simulated such a response to hairpin vortices using a power-law model, implying the hidden importance of the non-Newtonian property of deformable bubbles in drag reduction.

A further advanced question in regard to the rheological effect is the viscoelastic response of small bubbles. Since the shear rate fluctuates at a high frequency around individual bubbles in the turbulent boundary layer, the effective viscosity formulated for steady shear flow leads to misunderstanding. In general, the shear stress of a multiphase fluid element with a high interfacial area concentration is described by tensor equations as presented by Doi and Ohta (1991). For a dispersed bubble system, Llewellin and Manga (2005) proposed introducing the dynamic capillary number to describe the ratio of elastic to viscous contributions to the local shear stress. Murai and Oiwa (2008) confirmed with their falling-sphere viscometry that the effective viscosity increases drastically, departing from equilibrium deformation theory, as bubbles are subject to transient deformation. The experiment performed by Cui et al. (2003) showed 15 % drag reduction for a falling sphere in a highly turbulent regime of $Re > 10^4$. Decoding of their experimental condition matches the deformable bubble regime, which alters the turbulent boundary layer separation point on the sphere. For such viscoelasticity of bubbly liquid originating from surface tension, it is suggested that there is a need for more fundamental studies referring to the elastic resonance of bubbles in temporally fluctuating shear (Gao et al. 2011) and in a constraint environment (Prosperetti 2012). The momentum transfer from a stepwise accelerating wall measured by Sakurai et al. (2013) revealed a 60 % increment in effective viscosity with a void fraction of only 2 % as Ca unsteadily changed across unity. Figure 9 shows their sample data. The figure implies that such bubbles suppress turbulent eddies effectively; however, further investigation is required for a more generalized formulation. Relevant to this rheological effect, we should consider the phenomenological analogy to another type of drag reduction provided by a polymer surfactant solution such as that measured by Li et al. (2008).

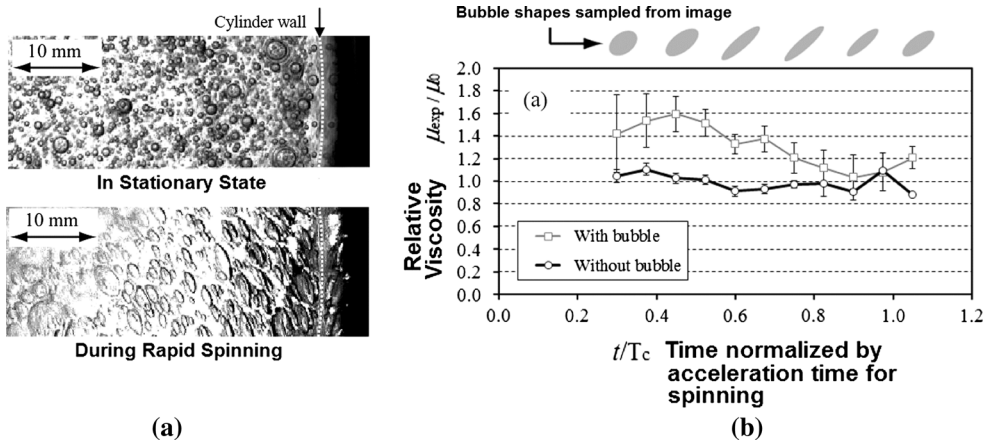

Fig. 9 Increase in the effective viscosity of bubbly liquid subject to transient bubble deformation. The two phases are air gas and highly viscous oil at room temperature, and fill a cylindrical container with a diameter of 145 mm. **a** *Top view* of bubble deformation near the wall owing to rapid spinning of the cylinder. **b** Effective viscosity at a point 10 mm from the wall, measured by ultrasound Doppler rheometry combined with a high-speed video camera system (Sakurai et al. 2013)

2.9 Fat bubbles comparable to the boundary layer thickness

Injection of fat bubbles into the liquid boundary layer beneath a horizontal wall greatly increases the friction coefficient. The resultant increases in wall shear stress overshadow the effect of reduced fluid density. Fat bubbles referred to here are bubbles sufficiently larger than the coherent structure of turbulence as they occupy most of the boundary layer thickness with their single diameter. Unlike an air cavity, the length in the streamwise direction is limited to a few times the boundary layer thickness. Their Weber number defined by Eq. (6) ranges from 10 to 300 in the air–water case, which is much larger than the critical Weber number for fragmentation in free shear flows. Such an effect was measured in a vertical channel by Liu (1997). The bubbles in his facility ranged between 5 and 15 mm in diameter, which was comparable to the boundary layer thickness. In horizontal flow beneath a wall, the fatness is maintained by buoyancy that keeps the bubbles stably beneath the wall. Numerical analysis of Kawamura and Kodama (2002) simulated the increase in wall shear stress owing to the bubbles that mostly occupy the boundary layer thickness. The finding of such a drag-increasing condition allows substantial improvement of drag reduction performance.

It is easily imaginable that fat bubbles moving along the wall force the ejection of liquid at their fronts and induce an extra sweep in their rears. In the case that the bubbles have significant slip velocity relative to the liquid, a similar additional momentum exchange occurs owing to their large volumes being subject to a steep velocity gradient. Oishi and Murai (2014) measured bubble-induced secondary flows around such fat bubbles in a turbulent channel flow as shown in Fig. 10. Four bubbles in the figure stably slide beneath the wall without temporal change to their shapes. The shape-fixing effect is provided by gravity; i.e., *Fr* number instead of the *We* number characterizes the shape. The liquid film flow that remains between the wall and bubble interface is governed by *Ca*: The top views of large bubbles accompany capillary waves. An important finding from their PTV is that the velocity fluctuation correlation $u'v'$ takes a value one order of magnitude higher than that of the original Reynolds shear stress in a single-phase boundary layer. The result explains consistently the loss of local skin friction reduction around large bubbles (Murai et al. 2007).

In the field of heat-transfer research, the role of such fat bubbles close to a wall has been investigated intensively. Fat bubbles, no matter of whether they comprise air or water vapor, promote turbulent heat transfer of the wall unless the bubbles entirely cover the wall to form an adiabatic sheet. A similar phenomenon for large bubbles is observed in laminar heat transfer (Kitagawa and Murai 2013) and laminar mass transfer. In laminar flow states, bubbles larger than the thermal and concentration boundary layer thicknesses provide pseudo-turbulent transport of the carrier phase. Such paradoxical experimental results between drag reduction and heat/mass transfer enhancement provide an analogous understanding of the role of large bubbles in the boundary layer.

2.10 Transition diagram of the drag reduction mechanism

As mentioned throughout this chapter, there are multiple scenarios of the effects of bubbles in drag reduction. The author does not explain them in complex detail, but each of

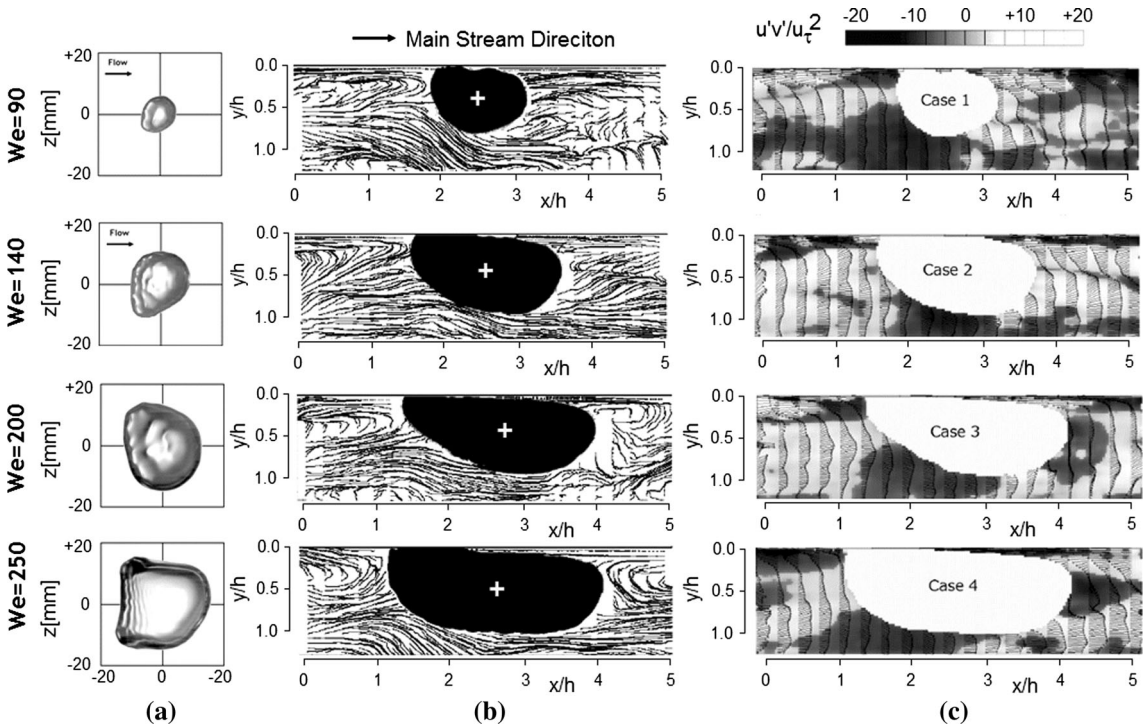

Fig. 10 Secondary flow patterns induced by fat bubbles co-currently migrating with liquid in a turbulent channel flow. **a** Typical *top-view* images of fat bubbles of four different sizes, **b** streamlines of the secondary flow component measured by PTV corresponding to each size, and **c** the spatial structure of the $u'v'$ distribution formed around each bubble where the value is scaled by the friction velocity squared (Oishi and Murai 2014)

them physically exists and has been experimentally demonstrated. Hence, we should remind ourselves that the simplest term "air-lubrication," which has been preferably used in the field of drag reduction for ships, is a grand generic term for an extremely complex combination of different mechanisms of drag reduction. Without such consideration, one would have an issue with the lack of experimental reproducibility for the void–drag relationship, which is a primary problem in application. In parallel, we need to appreciate that multiphase flows have their internally created deviations regardless of our strict control of the flow geometry and inlet bubble injection conditions.

What we can do in this situation is to make a rough classification of the local dominant mechanism in parameter space by clustering similar results. This work helps in practical design straggled between the multiplicity of the drag reduction mechanism and the inevitable deviating nature of bubbly two-phase flow. On the basis of this concept, a rough sketch of a drag reduction mechanism diagram is finally produced as shown in Fig. 11. The definition of the two-dimensional parameter space is the same as that for Fig. 4. The lines that separate the domain into seven regions are determined from experimental data. Thus, the lines can be termed as transition lines of the dominant drag reduction mechanism. It is noted that this diagram is approximately valid for horizontal turbulent boundary layers of water, but invalid for other flow configurations and other liquids such as highly viscous oil. Words within each region highlight the phenomenon relevant to drag reduction, and the value of G indicates the resultant mean gain factor [see Eq. (5)] realized in each region.

In the region "Spherical" at the bottom-left corner, frictional drag is in proportion to the effective viscosity of the spherical bubble mixture so that frictional drag increases in accordance with Eq. (11). The region "Yielding" on the right next is that for the use of highly deformable bubbles, in which drag reduction is restored by the bubble yielding effect. The theoretical gain factor is obtained as 5/3 as Ca goes to infinity in Eq. (12). Further large bubbles in slow two-phase flow transit to the region of "Gas film" because of buoyancy and provide drag reduction of $G = 1$.

The flow in the transition region from laminar to turbulent states ($0.1 < U < 1$ m/s) is sensitively affected by the injection of bubbles since bubbles perturb the laminar state and trigger the flow transition to turbulence (Huang et al. 2009). In most cases, therefore, bubbles rather activate the momentum transfer of the boundary layer so that drag increases. The same effect is known for free shear

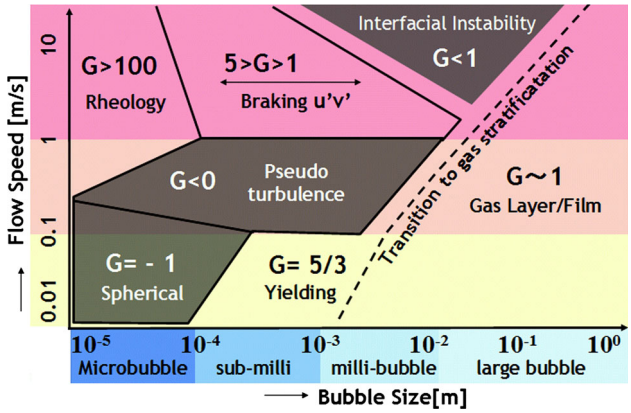

Fig. 11 Transition diagram of the drag reduction mechanism owing to bubble injection

flows and free-rising-bubble flows referred to as pseudo-turbulence or "turbulence" (Lance and Bataille 1991). The pseudoturbulence is decomposed into dipole-type potential disturbance and viscous wake disturbance. In either event, flow transition is promoted. This is a delicate problem especially in numerical simulation since it cannot be directly analyzed with a Eulerian formulation of volume-averaged equations (Kitagawa et al. 2001). On bubble-induced turbulence close to the wall, Kobe university group collected data of vertical two-phase flow systems, which give partial analogous discussion to that observed in horizontal systems. Hosokawa and Tomiyama (2013) found that Reynolds shear stress generated by bubble-induced pseudoturbulence was proportional to the ratio of void fraction to shear rate. A paper from their group, Ojima et al. (2014) clarified which terms in two-fluid formulation turbulent flow model take dominancy in describing bubble-induced turbulence.

Beyond the turbulent flow transition with an increase in flow speed, drag reduction revives as shown by the region "Braking $u'v'$" where the gain factor ranges from 1 to 5. Most cases of the so-called microbubble drag reduction for a ship belong to this region. Use of larger bubbles at the same flow speed causes a transition to "Interfacial instability" before stabilizing as a gas layer along the wall. In this region, bubbles subject to strong turbulent shear cannot keep their size due to active fragmentation and coalescence. The region "Rheology" at the top-left corner in the diagram has a high gain factor exceeding 100. Problems in this region are the considerable power required for microbubble generation and turbulent diffusion of microbubbles from the inner layer of the turbulent boundary layer.

The transition lines in the diagram shown here are simply presented to inspire researchers in the field and are not to be taken as universal absolutes. It is anticipated that the lines will be refined by further investigations.

3 Current problems and ideas

Together with the progress in understanding the drag reduction mechanism, limitations of the practical use of drag reduction are gradually emerging. They are (1) the short spatial persistency of the drag reduction effect for a large target like a vessel and (2) management of the rich unsteadiness that naturally occurs in the two-phase boundary layer. In response to the former problem, Kim and Cleaver (1995) proposed a simplified fitting function with which to estimate the persistency of drag reduction as a function of the gas flow rate. The function was such that drag reduction is always and fully lost far downstream. Main reason of the decline is bubbles' turbulent diffusion which will relax the peak void fraction near the wall. Sanders et al. (2006) investigated the downstream transition of bubble distribution along a 11-m-flat plate. They found that small bubbles at far downstream region behaved similarly to a passive scalar turbulent diffusion process (Poreh and Cermak 1964). This turns out the fact that bubbles no longer affect liquid phase there. However, gas–liquid two-phase flow confined in a thin turbulent boundary layer serves a further variety of flow patterns than we expect. Experiments in them give us many more ideas for the improvement, being challenged by many investigators. For instance, Elbing et al. (2008) found an abrupt transition from dispersed bubble state to gas layer structure, which jumps up local drag reduction ratio from 25 to 80 %. Thus, we have ample scope for improvement if we carefully observe the nature of two-phase flow. This chapter introduces and reviews ongoing research into the advances of drag reduction.

3.1 Bubbly Taylor–Couette flows

Shear flow generated in concentric annuli has been employed by several experimentalists in the fundamental study of bubble-originating drag reduction. The flow field is called Taylor–Couette flow (hereafter T–C flow). Its fluid dynamic characteristics have been richly explored for single-phase Newtonian fluid (Andereck et al. 1986; Takeda et al. 1994). Historically, T–C flow has long been investigated as a platform to elucidate scenarios of flow transition between laminar circular Couette flow and highly turbulent Couette flow (La Porta et al. 2001) starting with the onset of a Taylor vortex (Taylor 1923). Since the flow modes shift stepwise as the Reynolds number increases, the effect of bubble injection on the flow transition can be detected clearly. Another great advantage in using T–C flow is that the flow is organized in a spatial closure between two cylinders. Thereby, the momentum transfers can be assessed in a steady state under an ensured global energy balance. One can expect that the influence of

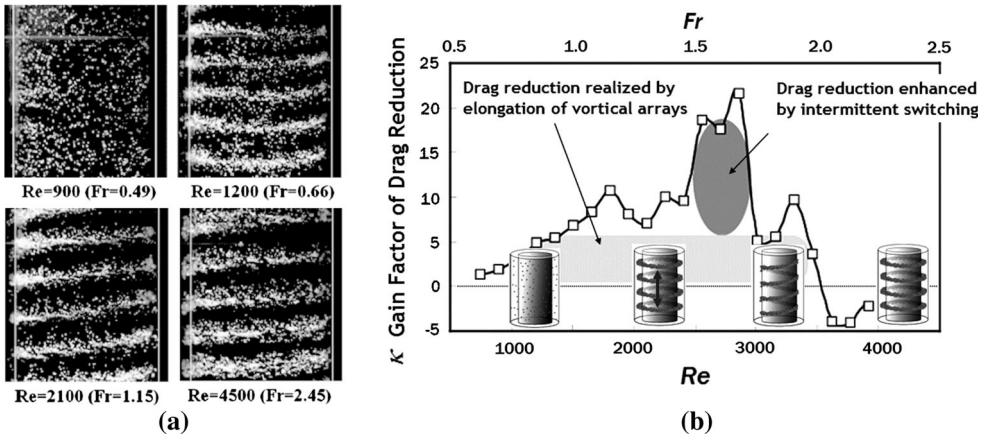

Fig. 12 Regularized bubble distribution and its effect on drag reduction in Taylor–Couette flow. Silicone oil and air are used as the two phases. No base axial flow is given to the liquid, while bubbles are continuously injected from the *bottom* at a fixed flow rate. **a** *Side view* of bubble distributions at different Reynolds numbers, showing random, toroidal, spiral, and turbulently diffused toroidal modes. **b** Gain factor of drag reduction changing with the mode switching of the bubble distribution pattern (Murai et al. 2008)

bubbles is exactly judged in the confined fluid shear from which no bubbles diffuse to escape. The idea contrasts the effect of bubbles with a spatially and temporally developing two-phase boundary layer either in a channel flow or from a flat wall. The comparison hints at how bubbles can reduce drag in a fully developed state, while several papers reported the priority of largely enhanced drag reduction during spatial development of the two-phase boundary layer (Xu et al. 2002).

The flow structure of bubbly T–C flow is classified by how the bubbles are mixed. Shiomi et al. (1993) measured bubble distribution patterns varying with the flow rates of two axially co-current phases. Atkhen et al. (2002) measured the phase velocity of the organized bubble distribution migrating with axial liquid flow. Air bubbles and cavitation bubbles were compared by Djeridi et al. (2004). Chemical engineers reported the enhancement of the gas–liquid interfacial area concentration by an array of vortical cells using horizontal-axis-type T–C flow (Hubacz and Wronski 2004). A variety of interfacial structures in the high gas volume fraction were also reported (Wronski et al. 2005; Mehal et al. 2007). In these two-phase flows, there cause air spots owing to bubble coalescence promoted by Taylor vortices and the centrifugal force of the rotating system. For relatively small bubbles, Climent et al. (2007) simulated preferential bubble accumulation to wavy vortical structures, which demonstrated the organized action of small bubbles on coherent structures for dilute bubble injection.

The actual performance of drag reduction in bubbly T–C flow was measured by two research groups: A group at the University of Twente investigated the highly turbulent regime, and a group at Hokkaido University focused on a weak turbulent regime. In the former case, van den Berg et al. (2005) and van den Berg et al. (2007) obtained a drag reduction of 20–25 % with a bulk mean void fraction of 4–8 % and *Re* from 10^5 to 10^6. They compared the drag reduction between small air bubbles and buoyant particles and ascertained that only air bubbles can achieve drag reduction. This clearly demonstrated that bubble deformability plays a major role in drag reduction in the highly turbulent regime. The latest study of van Gils et al. (2013) found a 40 % drag reduction with a 3 % void fraction by further increasing *Re* beyond 10^6. They witnessed that the promoted drag reduction originated from a shift in the Weber number from around unity to the order of 10. This scenario agrees with the work done by Kitagawa et al. (2005) for turbulent channel flows at a high Reynolds number. We are now reaching a conclusion that a steady drag reduction effect for turbulent shear flow having high *Re* number relies on bubble deformability.

For bubbly T–C flows at low Reynolds numbers, Murai et al. (2008) obtained 35 % drag reduction at *Re* of about 10^3 and a void fraction of 5 %. In this *Re* range, the Taylor vortex conveys momentum between the two cylinders, and vortex spacing and its topology were investigated by quantitative visualization of the inner structure. Their main finding was that bubbles increase the spacing between wavy traveling Taylor vortices so that drag is reduced. Sugiyama et al. (2008) simulated numerically such an interaction and found a collapse of the waves owing to spatially organized attack of spherical bubbles on the coherent structure. As the void fraction increases in this regime, the array of toroidal Taylor vortices shifts to spiral ones via emergence of the ellipsoidal instability of the Taylor vortex. The drag reduction performance per unit bubble buoyancy is a maximum in this topological transition regime as reported by Murai et al. (2008). Figure 12 shows a portion of their data. The internal two-phase flow

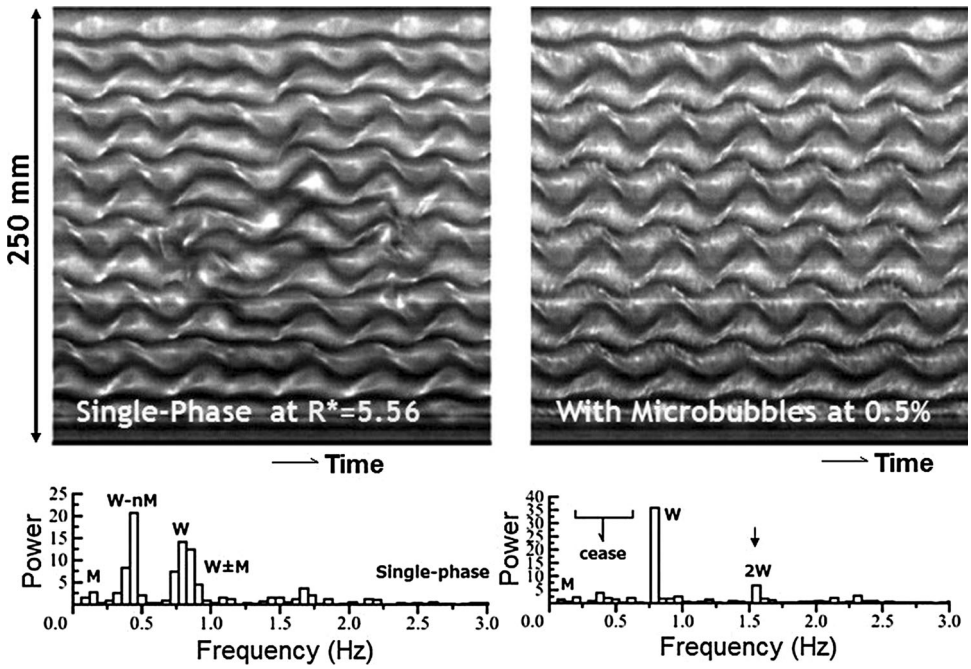

Fig. 13 Mode transition delayed by the dilute injection of microbubbles in Taylor–Couette flow. The *top two figures* show the spatiotemporal structure of the wavy Taylor vortex visualized by a Kalliroscope. The *bottom two* show the corresponding power spectra measured by ultrasound Doppler velocimetry

in such a transition regime was measured by Yoshida et al. (2009). They revealed global periodic switching between the toroidal and spiral modes, which naturally arises from the time lag between drag reduction and the formation of the corresponding bubble distribution pattern. Their group applied this interpretation to microbubbly T–C flow recently. As represented in Fig. 13, Watamura et al. (2013) found a delay in mode transition from the wavy Taylor vortex to the modulated one with the dilute injection of microbubbles. Their drag reduction in this regime reached 10 % with a void fraction of only 0.01 %. The bubble size dependent various trajectories in T–C flow were analyzed by Chouippe et al. (2014) based on Lagrangian approach. They elucidated the condition to cause a statistic preferential accumulation of bubbles subject to 3D turbulent shear flow. A curious data of using 3D bubble behavior was reported by Maryami et al. (2014). They observed combined improvement of drag reduction when microbubbles and axial flow were cooperatively imposed into vertical T–C flow.

Summarizing the drag reduction ascertained using T–C flow, three roles of bubbles are confirmed. In slow T–C flows, the buoyancy of bubbles alters the original T–C flow structure to totally different structures as gas–liquid two-phase flow. However, a dilute injection of bubbles works sufficiently well for drag reduction because the bubbles automatically structure the concentration spatially in accordance with vortical structures. This is known as the preferential concentration effect, which intensifies the bubble–liquid interaction in particular for unsteady vortical structures. For high-speed T–C flows, the effect of buoyancy becomes unimportant, and instead, bubble deformability supports a large drag reduction since length scales of coherent structures are shortened to less than the bubble size.

3.2 Effect of void waves and clustering

Bubbly two-phase flow more or less shows naturally induced fluctuation in the void fraction except in the cases of ideal inertia-less Stokes and Poiseuille flows. The question is how the spatiotemporal scale and the amplitude of such fluctuation affect the average drag reduction performance. The fluctuation originates from the relative motion of bubbles to the surrounding liquid. The term void wave expresses the propagation of the void fraction at a specific speed different from the bubble migration velocity. Compressibility of gas bubbles creates void waves together with pressure waves (Biesheuvel and van Wijngaaden 1984; Zhang and Prosperetti 1994). Since the speed of sound in bubbly liquid is dramatically lowered (roughly 30 m/s at a void fraction of 20 %), the bulk compressibility of bubbly mixture cannot be ignored in application to high-speed bubbly flows. For flow traveling faster than 10 m/s, the possibility of cavitation should also be considered (Ceccio 2010). The compressibility-induced void wave has an oscillatory wave front originating from the volumetric pulsation of the bubble (Kameda and Matsumoto 1996). As the resonance frequency of the pulsation falls in the band of the turbulent coherent structure, there is interaction

between them. The resonance frequency is known to be of the order of 100 kHz for a 1-mm air bubble in water at atmospheric pressure. It is, however, noted that the spherical volumetric pulsation of individual bubbles produces only irrotational velocity fluctuation in the liquid phase, and there has been no report of the importance of the pulsation in drag reduction, up to present.

Another factor triggering a void wave is the bubble's translational motion. The equation of motion of a single spherical bubble comprises seven force components. Details were reviewed by Michaelides (1997) and Magnaudet and Eames (2000). In monodispersed bubbly flow, the combination of these forces easily produces a spatially structured distribution of bubbles as a void wave. In the Stokes drag regime of bubble motion, bubbles in liquid turbulence tend to accumulate into the region where the second invariant of velocity gradient tensor is negative, while particles heavier than liquid accumulate into the positive region (Kitagawa et al. 2001). In sheared turbulence, a curious example of such intrinsic behaviors was analyzed by Tanaka (2013). He found that the Eulerian phase velocity of bubbles takes the inverse sign to the shearing direction. In bounded flows, the author's group found strong standing and pulsatile void waves in the buoyant rise of a bubble swarm close to a solid wall (Kitagawa et al. 2004; Kitagawa and Murai 2013, 2014). In a horizontal flow configuration, a similar integration of microbubbles to pulsatile migration was reported by Wu et al. (2007). They noted this effect as experimental fact when significant drag reduction was confirmed. Their following paper (Wu et al. 2008) analyzed which combination of parameters the most importantly dominates average drag reduction.

Bubble–bubble interaction is the third factor to take into account in the generation of void waves. This effect cannot be described by any treatment of the equation of motion for a single bubble. That is, the local liquid flows close to the bubble interface interact with each other as the distance between two bubbles decreases. In unbounded space, the interaction was analyzed by Sangani and Didwania (1993) and Seo et al. (2010) and measured by Brücker (1999) and Murai et al. (2006c). In vertical channel flows, local bubble clustering and its effect on near-wall turbulence was analyzed by Zenit et al. (2001) for spherical bubbles, and by Bunner and Tyggvason (2003) and Lu and Tryggvason (2007) for softly deformable bubbles. As plenty number of bubbles slide up along a vertical wall, bubble–bubble interaction was clearly observed in two dimensions (Kitagawa et al. 2004). In upward co-current bubbly channel flows, So et al. (2002) found intermittent swarms of sliding bubbles along the vertical walls as bubbles were nearly monodispersed. The generation of such sliding bubbles depends on the water-in surfactant which changes lift force acting on bubbles (Takagi et al. 2009). In short, the surfactant determines the emergence of bubble clustering near the wall in such a vertical system, and thereby affects the turbulent boundary layer (Takagi and Matsumoto 2011). This is one reason why measurements of drag reduction are sometimes diverse without the control of contamination.

The author's group is currently focusing on bubble–bubble interaction seen in horizontal wall boundary layers. Figure 14 shows a variety of bubble distribution patterns photographed from the top of a horizontal channel flow. The ordinate indicates a rough estimate of the projection of the void fraction defined by the wall-occupying ratio of bubbles. While this mapping of bubble clustering is still incomplete, it is immediately understandable that the bubble–turbulence interaction cannot be studied according to the motion of a single bubble. A random distribution can only be seen for the low void fraction in laminar flow. We observed lateral waves, streamwise chains, longitudinal clusters, slugging waves, and V-shaped clusters. Some migrate steadily and others show the dynamic and active exchange of bubbles between clusters. We also observed a uniform distribution for the high void fraction in a laminar flow state. The uniform distribution, which should be distinguished from a random distribution, means that bubbles strongly interact with repulsion forces for each neighbor. This is relevant to the observation made by Timkin and Gorelik (2010). They found homogeneously sliding bubbles in a vertical tube, which multiply the pipe wall friction in the transitional regime from laminar to turbulence. In turbulent flows, the photographs show streamwisely elongated void stripes that appear similar to what we know of the wall turbulence structure. A surprising feature of Fig. 14 is that there is less coalescence of bubbles inside the bubble cluster in highly turbulent regimes. This implies that the repulsive force intensifies during the rapid congregation of bubbles. Huang et al. (2009) measured modifications of sweep and ejection events through PIV and clarified that a bubble swarm more strongly suppresses actions than isolated bubbles. Oishi et al. (2009) measured the correlation between the passage of void waves and the local skin friction in a horizontal channel flow. Typical data are shown in Fig. 15. They found a time lag in the fluctuation between the two and ascertained that the time-averaged drag reduction was promoted as the void wave had large amplitude. This demonstrates that there is an intrinsic dynamic two-way interaction enhanced by the void waves along the wall. That is, a swarm of bubbles reduces local frictional drag around it, and the drag reduction affects the migration of the swarm. Park et al. (2009) examined the same effect using artificially generated void waves produced by the intermittent injection of bubbles. They obtained a gain of the drag reduction higher than that in the case without the intermittency, and their

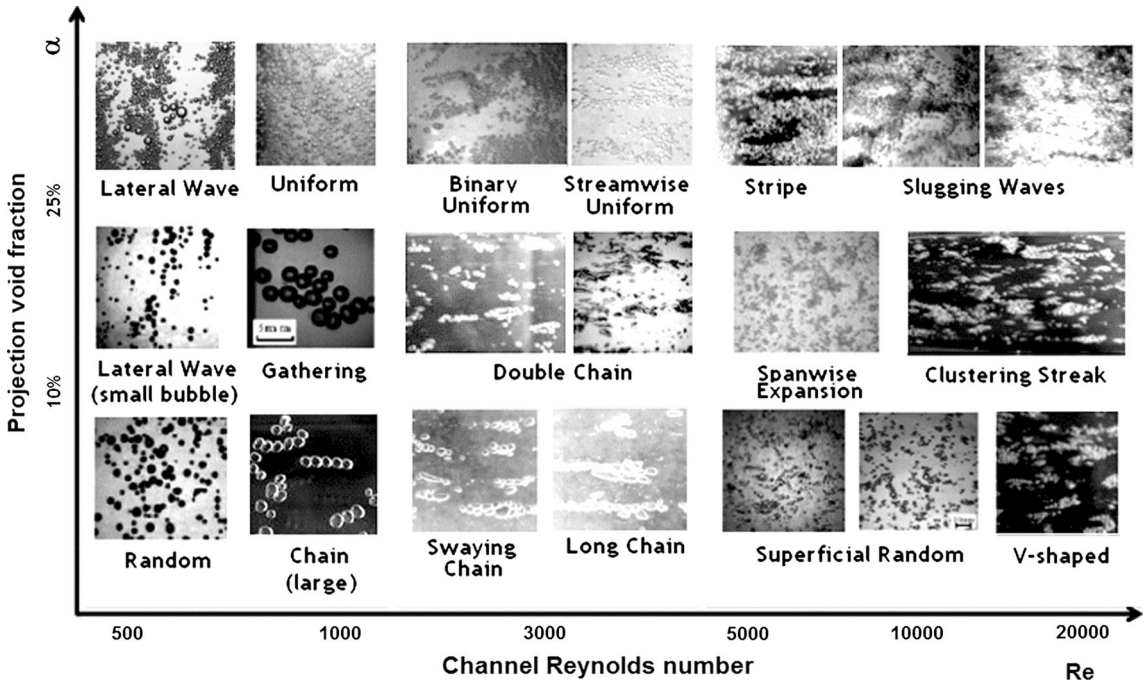

Fig. 14 Bubble distribution patterns photographed from the *top* of a horizontal turbulent channel flow. Silicone oil (5cSt) is used to avoid the contamination effect. The Reynolds number is defined by the half height of the channel and bulk mean velocity of the liquid. Image sizes vary and are 50 mm for local imaging and 160 mm in the largest case

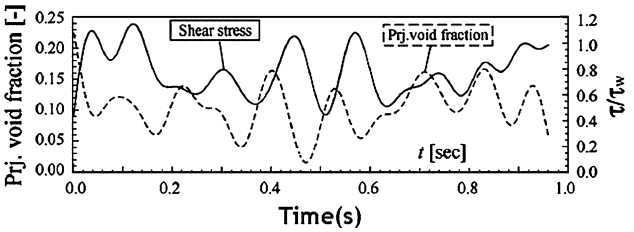

Fig. 15 Synchronized measurement of the local wall shear stress and local void fraction on the top wall of a horizontal bubbly channel flow. Both sensing areas are defined by a circle having a diameter of 20 mm, where bubbles of 0.5–1.5 mm pass by at about 1 m/s (Oishi et al. 2009)

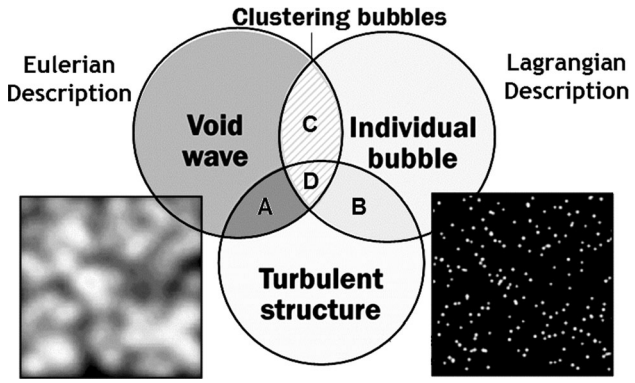

Fig. 16 Three kinds of two-way interaction considered in turbulent bubbly flow analysis

following paper reports how turbulent eddies are modified by each single passage of the void waves (Park et al. 2014). Macroscopically, a certain part of the void wave effect is explained by the discrepancy from the linearity of the drag reduction versus the average void fraction. The extra effect of the void waves could be attributed analogously to the compliant wall surface (Kramer 1960) and accelerating boundary layer (Piomelli and Yuan 2013) since void waves make the turbulent boundary layer thicker and thinner unsteadily.

To summarize this section, the analytical methodology for investigating the drag reduction mechanism is illustrated in Fig. 16. Three circles are drawn in the figure to define explicitly the role of bubble–bubble interaction. The overlapping regions of two circles indicate two-way interaction between the two elements. Overlap "A" can be analyzed employing a Eulerian–Eulerian two-phase flow approach such as the use of a two-fluid model, while the overlap "B" can be analyzed by taking a Eulerian–Lagrangian approach. Overlap "C" indicates bubble–bubble interaction that takes place when bubbles have a slip velocity relative to the liquid phase. The triple overlap of the three circles "D" is the future target of research toward a comprehensive understanding of the drag reduction mechanism, which also leads to an improvement in drag reduction performance.

3.3 Advances in measurement techniques

In the field of ship research, the overall measure of drag reduction performance is the reduction of the fuel consumption rate. For large vessels such as tankers and container carriers, turbulent frictional drag accounts for more than 70 % of total drag, and hence, a change owing to bubble injection is reflected in the shaft power for propulsion (Latorre 1997; Kumagai et al. 2010). In a towing experiment for a model ship and a flat plate, the towing force becomes a direct measure (Watanabe et al. 1998). In such research, the general relationship between the air injection flow rate and the resultant drag reduction was obtained for each type of ship hull as the cruising speed changes. The thickness of bubbly two-phase layer on the hull cannot be estimated accurately from these quantities while only the equivalent thickness of a gas film is inferred assuming that all the gas migrates along the wall at the same speed as the liquid phase. Even the mean void fraction in the boundary layer can hardly be approximated because it ordinarily has a steep profile as a function of the distance from the wall. Foeth et al. (2010) reported little effect of drag reduction in a series of full-scale vessel experiments using small bubbles. They explained this by bubbles escaping the boundary layer. To solve such an issue in application, a variety of measurement techniques have been developed to elucidate the two-phase flow characteristics as introduced below. The advance in measurement technique serves to bridge our fundamental understandings of the drag reduction mechanism and how practical applications should be designed.

Measurement of the void fraction is the most fundamental requirement for gas–liquid two-phase flow in any flow geometry. Optical probing is an existing technique that allows point-wise measurement of the void fraction. For turbulent channel flow, Guin et al. (1996) and Gabillet et al. (2002) adopted an optical fiber probe that traversed to measure the streamwise development of the vertical void fraction profile. Its advanced version realizes bubble-counting and bubble size measurement by mounting multiple apertures on its sensing head and combining with time-resolved signal processing (Luther et al. 2004; Higuchi and Saito 2010). For bubbly flows in a pipe, electrical capacitance tomography is recognized as a useful technology with which to approximately measure the cross-sectional void fraction distribution (e.g., Warsito and Fan 2001). In contrast, a wire-mesh sensor installed inside a pipe allows direct measurement of the phase distribution (Prasser et al. 2001). Its extension to bubbly channel flow was presented by Richter et al. (2002). They succeeded in simultaneous measurements of the transient void fluctuation, bubble size, and bubble velocity by means of a well-devised spatial arrangement of the wire mesh.

Digital image processing is widely employed in bubbly flow measurement in two dimensions. Moriguchi and Kato (2002) analyzed a bubble interfacial image illuminated by a laser sheet to measure the void fraction profile close to the wall in a horizontal channel flow. Backlighting of bubbles provides clear shadow images so that the shape information of bubbles is simultaneously obtained as applied by Fujiwara et al. (2004) for a vertical bubbly channel flow. While a single view of backlight bubble imaging is limited to dilute bubbly flow, stereoscopic imaging allows measurement of the three-dimensional void fraction. Statistic and deterministic methods were proposed by Murai et al. (2001), and Luo et al. (2002), respectively. For bubbles in laser illumination, Kawaguchi et al. (2002) proposed the use of interference fringes converted to a one-dimensional stripe pattern for bubble detection and size measurement. Its combined use with PIV was realized for spraying phenomena (Hardalupas et al. 2010), which is expected to be applied to microbubbly turbulent flows. For vertical bubbly pipe flows, Lelouvetel et al. (2014) has successfully extracted turbulent cascade process altered by bubbles by means of PTV combined with bubble-shape projection imaging technique.

For gas–liquid two-phase flow of highly concentrated gas–liquid interfaces, radiation type visualization works instead of the above-mentioned optical approach. X-ray measurement instrumentation is designable since it is attenuated in liquid phase, but insignificant in gas phase. Stutz and Legoupil (2003) sandwiched a high-speed Venturi throat by the source and the detector of X-ray and successfully measured oscillating cloud-state cavitation bubbles at 1 kHz in sampling frequency. For two-phase flow in a circular tube, many pairs of the X-ray sources and detectors can be arranged in the angular direction to realize computed tomographic visualization as presented by Fischer and Hampel (2010). The application to a partial cavity flow was recently reported by Mäkiharju et al. (2013a, b). They constructed a two-dimensional X-ray densitometry system which can acquire the void image at 1 kHz and successfully explored the internal unsteady void profile as a function of distance from the wall.

Ultrasound senses bubbles from the differential acoustic impedances of two phases and has long been an alternative to optical techniques. Amplitude modification of reflected ultrasound is used in medical instruments where encapsulated microbubbles are injected into blood vessels as an ultrasonic contrast agent. For the detection of bubbles in a flowing state, the ultrasonic Doppler shift (thus frequency modification) also provides the interfacial location as developed by the author's group (Murai et al. 2006a, 2010). In its application, void fraction profiles of a bubbly turbulent boundary layer were successfully measured. Figure 17 shows sample data from Murai et al. (2009).

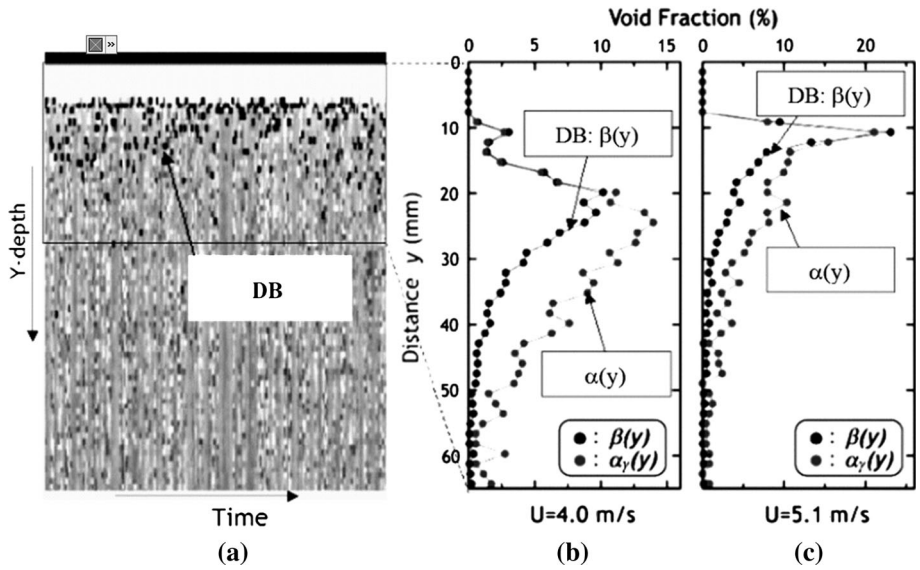

Fig. 17 Ultrasound Doppler sensing of bubbles applied to the turbulent boundary layer formed beneath a long flat-towed plate with the injection of bubbles. **a** Detected bubbles marked in black in spatiotemporal Doppler shift information. **b** Wall-perpendicular profile of detected bubbles $\beta(y)$ and reconstructed void fraction profile $\alpha(y)$ at a towing speed of $U = 4.0$ m/s. The measurement section is 25-m downstream of the bubble injector. **c** The same profiles at $U = 5.1$ m/s (Murai et al. 2009)

The signal of the bubble interface ("DB" in the figure) on the map of the Doppler shift frequency is spatially integrated with a convolution function to obtain the short-time average void fraction profile as a function of distance from the wall. The profiles are those beneath a long horizontal flat plate towed in stationary water at the National Maritime Research Institute (NMRI-Japan). The data show a shift in the void peak toward the wall as the towing speed increases. Recent progress of the ultrasonic Doppler method for fluid flow measurement was summarized in Springer's book edited by Takeda (2012).

Measurement of liquid velocity distributions in bubbly turbulent boundary layers might be the most laborious work. Gabillet et al. (2002) developed hot-wire anemometry for measurement of the liquid-phase velocity. They raised the sampling frequency to 20 kHz so that each passage of bubbles of a few millimeters was detected from the sudden drop in the output voltage owing to the lower thermal conductivity inside bubbles. They introduced two thresholds into data processing to discriminate bubbles from the velocity fluctuation of turbulent flow. Another discrimination for hot-wire anemometry was proposed by Rensen et al. (2005a) and applied to a bubbly flow (Rensen et al. 2005b). LDV applicable to bubbly turbulent flow was proposed by So et al. (2002). They modified the optical geometry of a commercial two-color LDV system so that laser beams detour about bubbles that accumulated inside turbulent boundary layers.

PIV requires image separation into two phases, prior to or during the digital image processing. For bubbly turbulent channel flows, infrared shadow imaging for bubbles was combined with PIV by Fujiwara et al. (2004), and the same with particle tracking velocimetry (PTV) by Kitagawa et al. (2005). To prevent irregular light scattering about deformable bubbles, Huang et al. (2008) proposed a shallowly set depth-of-focus (DOF) for backlighting PTV. They measured bubble-induced velocity fluctuation within a DOF-defined layer close to the wall. Figure 18 shows their samples, depicted by in-plane divergence of the measured velocity vector field within 30 wall units from the wall. The sink and source are recognized clearly in the downstream and upstream regions of bubbles, respectively. Since the pair of sink and source corresponds with ejection and sweep events along the wall, it was ascertained with spectral analysis that only small bubbles modify the coherent structures. The DOF-narrowing technique was extended by Murai et al. (2006b) for flow in the wall-perpendicular direction. With a very different approach from the above, Hosokawa et al. (2009) realized the near-wall turbulent flow characterization of bubbly flow in a square duct by means of molecular tagging velocimetry. They performed photo-bleaching reactions in liquid phase on a microscale and successfully measured the velocity gradient tensors in a turbulent bubbly flow. Their following paper (Hosokawa and Tomiyama (2013)) succeeded in validating Reynolds-averaged model for bubbly flows with the data obtained by the same technique.

Summarizing this chapter, the author himself relearned that the ideas for measurement tools lead to discoveries relating to the drag reduction mechanism. In opposing direction, our continuous and enthusiastic effort to understand the fundamental physics propels the development of measurement techniques. As mentioned in Sects. 3.1 and 3.2, advances in understanding provide the next questions to answer. The main feature of Sect. 3.3 is that the spatiotemporal resolving of measurements of the bubbly turbulent boundary layer demonstrates the ample scope for improvement of drag reduction performance. At the same

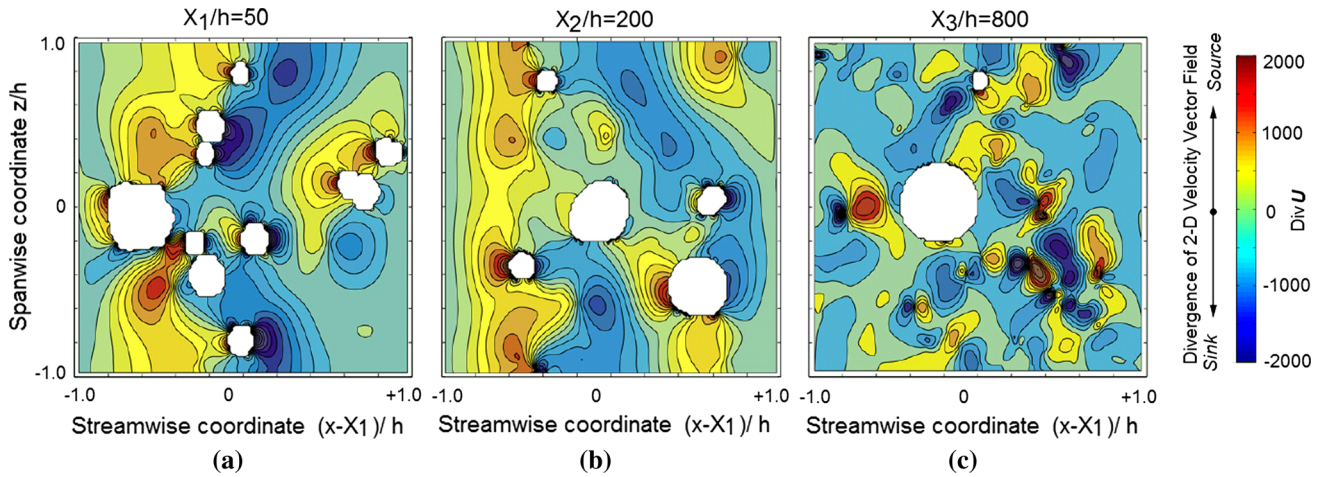

Fig. 18 Liquid velocity fluctuation induced by bubbles of various sizes in the wall proximity of a horizontal turbulent channel flow. The bulk mean liquid velocity is $U = 2$ m/s ($Re = 8{,}800$), flowing from *left* to *right* in each figure (100 × 100 mm). The bubble size has a Gaussian distribution centered at 1.0 mm with a standard deviation of 0.5 mm. The two-dimensional divergence of velocity vector field at 1.50 ± 0.15 mm from the wall is visualized in color for three measurement sections: **a** 250 mm, **b** 1 m, **c** 4 m from the bubble injection point (Huang et al. 2008)

time, the lack of reproducibility, which has long been a concern to experimentalists, is close to the solution. Consequently, the author can say that it is finally time to test our new ideas in application devices based on historically integrated knowledge stated in this article.

4 Conclusions

Drag reduction by bubble injection was reviewed. In contrast to past review papers such as that by Merkle and Deutsch (1990), the present review highlights the great progress made in regard to "understanding" the internal mechanism of the drag reduction. The progress relies on recent advances in measurement techniques that have been established to resolve complex bubbly two-phase flow structures subject to strong turbulence. In particular, the importance placed on fundamental research using channel flows and circular Couette flows has led to a hot discussion on the interpretation of the roles of a bubble's slip velocity and the interfacial deformability in turbulence. In a spatially developing boundary layer, the slip plays the principal role in modifying the turbulent shear stress field. The deformability maintains drag reduction in fully developed turbulence and contributes to the insensitivity to the bubble size once bubbles start to deform. The rheology of bubbly liquid in a wide dynamic range of the shear rate showed strong non-Newtonian properties affecting all regimes from laminar to highly turbulent states. Namely, the mechanism of drag reduction is little explained by a single universal hypothesis, but has been classified into multiple regions in the parameter space of our interest. This is not unfortunate since we already learned that gas–liquid two-phase flow just in a circular pipe comprises several very different flow patterns. In contrast, some experimentalists discovered highly organized interaction between two phases as the bubbles are controlled to be nearly spherical and monodispersed. The use of such bubbles quite often induces naturally forming void waves owing to the interphase interaction regularized in the time–space domain. The authors expect that these phenomena will be potentially contributable to the next advance in drag reduction through bubble injection.

Acknowledgments The author would like to thank Prof. Koichi Hishida and Dr. Yoshihiko Oishi for their assistance in preparing this manuscript, and also Prof. Hiroharu Kato and Dr. Yuji Tasaka for their long support relating to this topic. The work of the author's group in the manuscript was supported by the Ministry of Education, Science, Sports and Culture, Japan, a Grant-in-Aid for Scientific Research (KAKENHI Grant Numbers 24246033 and 21360077), and also financially supported by the New Energy Development Organization, Japan (NEDO Project Number 08B36002d). The author expresses thanks for this support.

References

Adrian RJ (2007) Hairpin vortex organization in wall turbulence. Phys Fluids 19:041301

Aliseda A, Lasheras JC (2006) Effect of buoyancy on the dynamics of a turbulent boundary layer laden with microbubbles. J Fluid Mech 559:307–334

Amromin E, Mizine I (2003) Partial cavitation as drag reduction technique and problem of active flow control. Mar Technol 40:181–188

Amromin E, Karafiath G, Metcalf B (2011) Ship drag reduction by air bottom ventilated cavitation in calm water and in waves. J Ship Res 55:196–207

Andereck CD, Liu SS, Swinny HL (1986) Flow regimes in a circular Couette system with independently rotating cylinders. J Fluid Mech 164:155–183

Atkhen K, Fontaine J, Wesfreid JE (2002) Highly turbulent Couette–Taylor bubbly flow patterns. J Fluid Mech 422:55–68

Batchelor GK (1967) Effective viscosity of dilute dispersion: an introduction to fluid dynamics. Cambridge University Press, Cambridge, pp 246–255

Biesheuvel A, van Wijngaaden L (1984) Two-phase flow equations for a dilute dispersion of gas bubbles in liquid. J Fluid Mech 148:301–318

Boffetta G, Celani A, Vergassola M (2000) Inverse energy cascade in two-dimensional turbulence: deviations from Gaussian behavior. Phys Rev E 61:29–32

Brücker C (1999) Structure and dynamics of the wake of bubbles and its relevance for bubble interaction. Phys Fluids 11:1781–1796

Bunner B, Tryggvason G (2003) Effect of bubble deformation on the properties of bubbly flow. J Fluid Mech 495:77–118

Callenaere M, Franc JP, Michel JM, Riondet M (2001) The cavitation instability induced by the development of a re-entrant jet. J Fluid Mech 444:223–256

Ceccio S (2010) Frictional drag reduction of external flows with bubble and gas injection. Annu Rev Fluid Mech 42:183–203

Chouippe A, Climent E, Legendre D, Gabillet C (2014) Numerical simulation of bubble dispersion in turbulent Taylor–Couette flow. Phys Fluids 26:043304

Climent E, Simonnet M, Magnaudet J (2007) Preferential accumulation of bubbles in Couette–Taylor flow patterns. Phys Fluids 19:083301

Crowe CT, Troutt TR, Chung JN (1996) Numerical models for two-phase turbulent flows. Annu Rev Fluid Mech 28:11–43

Cui Z, Fan JM, Park AH (2003) Drag coefficients for a settling sphere with microbubble drag reduction effects. Power Technol 138:132–134

Djeridi H, Gabillet C, Billard Y (2004) Two-phase Couette–Taylor flow: arrangement of the dispersed phase and effect on the flow structure. Phys Fluids 16:128–139

Doi M, Ohta T (1991) Dynamics and rheology of complex interfaces I. J Chem Phys 95(2):1242–1247

Dominguez-Lerma MA, Ahlers G, Channell DS (1985) Effects of Kalliroscope flow visualization particles on rotating Couette–Taylor flow. Phys Fluids 28:1204–1206

Einstein A (1906) Eine neue Bestimmung der Molekuldimensionen. Ann Phys 19:289–306

Elbing BR, Winkel ES, Lay KA, Ceccio SL, Dowling DR, Perlin M (2008) Bubble-induced skin-friction drag reduction and the abrupt transition to air-layer drag reduction. J Fluid Mech 612:201–236

Elbing BR, Mäkiharju S, Wiggins A, Perlin M, Dowling DR, Ceccio SL (2013) On the scaling of air layer drag reduction. J Fluid Mech 717:484–513

Felton K, Loth E (2001) Spherical bubble motion in a turbulent boundary layer. Phys Fluids 13:2564–2577

Felton K, Loth E (2002) Diffusion of spherical bubbles in a turbulent boundary layer. Int J Multiph Flow 28:69–92

Ferrante A, Elghobashi S (2004) On the physical mechanism of drag reduction in a spatially developing turbulent boundary layer laden with microbubbles. J Fluid Mech 503:345–355

Ferrante A, Elghobashi S (2005) Reynolds number effect of drag reduction in a microbubble-laden spatially developing turbulent boundary layer. J Fluid Mech 543:93–106

Fischer F, Hampel U (2010) Ultra fast electron beam X-ray computed tomography for two-phase flow measurement. Nuclear Eng Des 240(9):2254–2259

Foeth EJ, Eggers R, Quadvlieg EHHA (2010) The efficiency of air-bubble lubrication for decreasing friction resistance. Prof. int. conf. ship drag reduction (SMOOTH-SHIPS), Instanbul, Turkey. Paper No. 12, pp 9

Frankel NA, Acrivos A (1970) The constitutive equation for a dilute emulsion. J Fluid Mech 44:65–78

Fujikawa S, Yano Y, Watanabe M (2011) Vapor–liquid interfaces, bubbles and droplets: fundamentals and applications. Series of heat and mass transfer. Springer, Berlin

Fujiwara A, Minato D, Hishida K (2004) Effect of bubble diameter on modification of turbulence in an upward pipe flow. Int J Heat Fluid Flow 25:481–488

Fukagata K, Iwamoto K, Kasagi N (2002) Contribution of Reynolds stress distribution to the skin friction in wall-bounded flows. Phys Fluids 14:L73–L76

Fukuda K, Tokunaga J, Nobunaga T, Nakatani T, Iwasaki T (2000) Frictional drag reduction with air lubricant over a super-water-repellent surface. J Mar Sci Technol 5:123–130

Gabillet C, Colin C, Fabre J (2002) Experimental study of bubble injection in a turbulent boundary layer. Int J Multiph Flow 28:553–578

Gao T, Hu HH, Castaneda PP (2011) Rheology of a suspension of elastic particles in a viscous shear flow. J Fluid Mech 687:209–237

Gore RA, Crowe CT (1989) Effect of particle size on modulating turbulent intensity. Int J Multiph Flow 15:279–285

Gore RA, Crowe CT (1991) Modulation of turbulence by a dispersed phase. J Fluids Eng 113:304–307

Guin MM, Kato H, Yamaguchi H, Maeda M, Miyanaga M (1996) Reduction of skin friction by microbubbles and its relation with near wall bubble concentration in a channel. J Mar Sci Technol 1:241–254

Hara K, Suzuki T, Yamamoto F (2011) Image analysis applied to study on frictional drag reduction by electrolytic microbubbles in a turbulent channel flow. Exp Fluids 50:715–727

Hardalupas A, Sahu S, Taylor AMKP, Zarogoulidis K (2010) Simultaneous planer measurement of droplet velocity and size with gas phase velocities in a spray by combined ILIDS and PIV techniques. Exp Fluids 49:417–434

Hassan YA, Ortiz-Villafuerte J (2003) Investigation of microbubble boundary layer using particle image velocimetry. In: Proceedings of ASME FEDSM'03 -45639 [CD-ROM], Fourth ASME-JSME Joint Fluids Engineering Conference, Honolulu, HI

Hassan YA, Gutierrez Torres CC, Jimenez-Bernal JA (2005) Temporal correlation modification by microbubbles injection in a channel flow. Int Commun Heat Mass Transf 32:1009–1015

Hesketh RP, Etchells AW, Russell TWF (1991) Bubble breakage in pipeline flow. Chem Eng Sci 46:1–9

Higuchi M, Saito T (2010) Quantitative characterizations of long-period fluctuations in a large-diameter bubble column based on point-wise void fraction measurements. Chem Eng J 160:284–292

Hinze JO (1955) Fundamentals of the hydrodynamic mechanism of splitting in dispersion processes. AIChE J 1:289–295

Hirata M, Nishiwaki N (1963) Skin friction and heat transfer for liquid flow over a porous wall with gas injection. Int J Heat Mass Transf 6:941–949

Hosokawa S, Tomiyama A (2004) Turbulence modification in gas–liquid and solid–liquid dispersed two-phase pipe flows. Int J Heat Fluid Flow 25:489–498

Hosokawa S, Tomiyama A (2009) Multi-fluid simulation of turbulent bubbly pipe flows. Chem Eng Sci 64:5308–5318

Hosokawa S, Tomiyama A (2013) Bubble-induced pseudo turbulence in laminar pipe flows. Int J Heat Fluid Flow 40:97–105

Hosokawa S, Fukunaga T, Tomiyama (2009) Application of photobleaching molecular tagging velocimetry to turbulent bubbly flow in a square duct. Exp Fluids 47:745–754

Huang J, Murai Y, Yamamoto F (2008) Shallow DOF-based particle tracking velocimetry applied to horizontal bubbly wall turbulence. Flow Meas Instrum 19:93–105

Huang J, Murai Y, Yamamoto F (2009) Quadrant analysis of bubble induced velocity fluctuation in a transitional boundary layer. J Hydrodyn 21:93–99

Hubacz R, Wronski S (2004) Horizontal Couette–Taylor flow in a two-phase gas–liquid system: flow patters. Exp Therm Fluid Sci 28:457–472

Ishii M, Hibiki T (2011) Drift-flux model: thermo-fluid dynamics of two-phase flow. Springer, Berlin

Iwasaki T, Nishimura K, Tanaka M, Hagiwara Y (2001) Direct numerical simulation of turbulent Couette flow with immiscible droplets. Int J Heat Fluid Flow 22:332–342

Jacob B, Olivieri A, Miozzi M, Campana EF, Piva R (2010) Drag reduction by microbubbles in a turbulent boundary layer. Phys Fluids 22:115104

Jimenez J (2012) Cascades in wall-bounded turbulence. Annu Rev Fluid Mech 44:27–45

Kameda M, Matsumoto Y (1996) Shock waves in a liquid containing small gas bubbles. Phys Fluids 8:322–335

Kato H, Iwashina T, Miyanaga M, Yamaguchi H (1999) Effect of microbubbles on the structure of turbulence in a turbulent boundary layer. J Mar Sci Technol 4:115–162

Katsui T, Okamoto Y, Kasahara Y, Shimoyama N, Iwasaki Y, Soejima S (2003) A study of air lubrication method to reduce frictional resistance of ship: experimental investigation by tanker form model ship and estimation of full scale ship performance. J Kansai Soc Nav Archit Jpn 239:45–53 (in Japanese)

Kawaguchi T, Akasaka Y, Maeda M (2002) Size measurement of droplets and bubbles by advanced interferometric laser imaging technique. Meas Sci Technol 13:308

Kawamura T, Kodama Y (2002) Numerical simulation method to resolve interactions between bubbles and turbulence. Int J Heat Fluid Flow 23:627–638

Kim J (2003) Control of turbulent boundary layers. Phys Fluids 15:1093–1106

Kim SY, Cleaver JW (1995) The persistence of drag reduction following the injection of microbubbles into a turbulent boundary layer. Int Commun Heat Mass Transf 22:353–357

Kitagawa A, Murai Y (2013) Natural convection heat transfer from a vertical heated plate in water with microbubble injection. Chem Eng Sci 99:215–224

Kitagawa A, Murai Y (2014) Pulsatory rise of microbubble swarm along a vertical wall. Chem Eng Sci 116:694–703

Kitagawa A, Murai Y, Yamamoto F (2001) Two-way coupling of Eulerian–Lagrangian model for dispersed multiphase flows using filtering functions. Int J Multiph Flow 27:2129–2153

Kitagawa A, Sugiyama K, Murai Y (2004) Experimental detection of bubble–bubble interactions in a wall-sliding bubble swarm. Int J Multiph Flow 30:1213–1234

Kitagawa A, Hishida K, Kodama Y (2005) Flow structure of microbubble-laden turbulent channel flow measured by PIV combined with the shadow image technique. Exp Fluids 38:466–475

Kitagawa A, Kosuge K, Uchida K, Hagiwara Y (2008) Heat transfer enhancement for laminar natural convection along a vertical plate due to sub-millimeter-bubble injection. Exp Fluids 45:473–484

Kodama Y, Kakugawa A, Takahashi T, Kawashima H (2000) Experimental study on microbubbles and their applicability to ships for skin friction reduction. Int J Heat Fluid Flow 21:582–588

Kramer MO (1960) Boundary layer stabilization by distributed damping. J Am Soc Nav Eng 72:25–34

Kulick JD, Fessler JR, Eaton JK (1994) Particle response and turbulence modification in fully developed channel flow. J Fluid Mech 277:109–134

Kumagai, I, Nakamura N, Murai Y, Tasaka Y, Takeda Y, Takahashi Y (2010) A new power-saving device for air bubble generation: hydrofoil air pump for ship drag reduction. In: Proceedings of international conference on ship drag reduction, Istanbul (Smooth), pp 95–102

Kwon BH, Kim HH, Jeon HJ, Kim MC, Lee I, Chun S, Go JS (2014) Experimental study on the reduction of skin frictional drag in pipe flow by using convex air bubbles. Exp Fluids 55:1772

L'vov VS, Pomyalov A, Procaccia I, Tiberkevich V (2005) Drag reduction by microbubbles in turbulent flows: the limit of minute bubbles. Phys Rev Let 94:174502

La Porta A, Voth GA, Crawford AM, Alexander J, Bodenschatz E (2001) Fluid particle accelerations in fully developed turbulence. Nature 409:1017–1019

Lance M, Bataille J (1991) Turbulence in the liquid phase of a uniform bubbly air–water flow. J Fliud Mech 222:95–118

Latorre R (1997) Ship hull drag reduction using bottom air injection. Ocean Eng 24:161–175

Latorre R, Miller A, Philips R (2003) Micro-bubble resistance reduction on a model SES catamaran. Ocean Eng 30:2297–2309

Lay KA, Yakushiji R, Makiharju S, Perlin M, Ceccio SL (2010) Partial cavity drag reduction at high Reynolds number. J Ship Res 54:109–119

Lee CY, Kim CJ (2011) Underwater restoration and retention of gases on superhyrdophibic surfaces for drag reduction. Phys Rev Lett 106:014502

Legner HH (1984) Simple model for gas bubble drag reduction. Phys Fluids 27:2788–2790

Lelouvetel J, Tanaka T, Sato Y, Hishida K (2014) Transport mechanisms of the turbulent energy cascade in upward/downward bubbly flows. J Fluid Mech 741:514–542

Li FC, Kawaguchi Y, Yu B, Wei JJ, Hishida K (2008) Experimental study of drag-reduction mechanism for a dilute surfactant solution flow. Int J Heat Mass Transf 51:835–843

Liu TJ (1997) Investigation of the wall shear stress in vertical bubbly flow under different bubble size conditions. Int J Multiph Flow 23:1085–1109

Llewellin EW, Manga M (2005) Bubble suspension rheology and implications for conduit flow. J Volcanol Geotherm Res 143:205–217

Lockhart RW, Martinelli RC (1949) Proposed correlation of data for isothermal two-phase two-component flow in pipes. Chem Eng Process 45:39–48

Lu J, Tryggvason G (2007) Effect of bubble size in turbulent bubbly downflow in a vertical channel. Chem Eng Sci 62:3008–3018

Lu J, Fernandez A, Tryggvason G (2005a) The effect of bubbles on the wall drag in a turbulent channel flow. Phys Fluids 17(095102):1–12

Lu X, Hamada M, Kato H (2005b) Effect of the turbulent frictional drag reduction of microbubbles: experiments by bubbles of air and hydrogen. In: Proc. fluid eng. conf. of Japan soc. mech. eng. (JSME), Paper No. 509:69–70

Lundin MD, McCready MJ (2009) Modeling of bubble coalescence in bubbly co-current flows restricted by confined geometry. Chem Eng Sci 64:4060–6067

Luo R, Song Q, Yang XY, Wang Z (2002) A three-dimensional photographic method for measurement of phase distribution in dilute bubble flow. Exp Fluids 32:116–120

Luther S, Rensen J, Guet S (2004) Bubble aspect ratio and velocity measurement using a four-point fiber-optical probe. Exp Fluids 36:326–333

Madavan NK, Deutsch S, Merkle CL (1985) Measurements of local skin friction in microbubble-modified turbulent boundary layer. J Fluid Mech 156:237–256

Magnaudet J, Eames I (2000) The motion of high-Reynolds-number bubbles in inhomogeneous flows. Annu Rev Fluid Mech 32:659–708

Mäkiharju SA, Perlin M, Ceccio SL (2012) On the energy economics of air lubrication drag reduction. Int J Nav Archit Ocean Eng 4(4):412–422

Mäkiharju SA, Elbing BR, Wiggins A, Schinasi S, Vanden-Broeck JM, Perlin M, Ceccio SL (2013a) On the scaling of air entrainment from a ventilated partial cavity. J Fluid Mech 732:47–76

Mäkiharju SA, Gabillet C, Paik BG, Chang NA, Perlin M, Ceccio SL (2013b) Time-resolved two-dimensional X-ray densitometry of a two-phase flow downstream of a ventilated cavity. Exp Fluids 54(7):1561

Marie JL (1987) A simple analytical formulation for microbubble drag reduction. J PhysicoChem Hydrodyn 13:213–220

Maryami R, Farahat S, Poor MJ, Mayam MHS (2014) Bubbly drag reduction in a vertical Couette–Taylor system with superimposed axial flow. Fluid Dyn Res 46:055504. doi:10.1088/0169-5983/46/5/05504

Masliyah J, Jauhari R, Gray M (1994) Drag coefficient for air bubbles rising along an inclined surface. Chem Eng Sci 49:1905–1911

Matveev KI (2007) Three dimensional wave patterns in long air cavities on a horizontal plane. Ocean Eng 34:1882–1891

Maxey MR, Chang EJ, Wang LP (1996) Interaction of particles and microbubbles with turbulence. Exp Therm Fluid Sci 12:417–425

McCormick M, Bhattacharyya R (1973) Drag reduction of a submersible hull by electrolysis. Nav Eng J 85:11–16

Mehel A, Gabillet C, Djeridi H (2007) Analysis of the flow pattern modifications in a bubbly Couette–Taylor flow. Phys Fluids 19:118101

Merkle CL, Deutsch S (1990) Drag reduction in liquid boundary layers by gas injection. Prog Astronaut Aeronaut 123:351–411

Merkle CL, Deutsch S (1992) Microbubble drag reduction in liquid turbulent boundary layers. ASME Appl Mech Rev 45:103–127

Michaelides EE (1997) The transient equation of motion for particles, bubbles, and droplets. J Fluids Eng 119:233–247

Michel JM (1984) Some features of water flows with ventilated cavities. J Fluid Eng 106(3):319–326

Mizokami S, Kawakita C, Kodan Y, Takano S, Higasa S, Shigenaga R (2010) Experimental study of air lubrication method and verification of effects on actual hull by means of sea trial. Mitsubishi Heavy Ind Techn Rev 47(3):41–47

Moctezuma MF, Lima-Ochoterena R, Zenit R (2005) Velocity fluctuations resulting from the interaction of a bubble with a vertical wall. Phys Fluids 17:098106

Moriguchi Y, Kato H (2002) Influence of microbubble diameter and distribution on frictional resistance reduction. J Mar Sci Technol 7:79–85

Murai Y, Oiwa H (2008) Increase of effective viscosity in bubbly liquids from transient bubble deformation. Fluid Dyn Res 40:565–575

Murai Y, Matsumoto Y, Yamamoto F (2001) Three-dimensional measurement of void fraction in a bubble plume using statistic stereoscopic image processing. Exp Fluids 30:11–21

Murai Y, Oishi Y, Sasaki T, Kodama Y, Yamamoto F (2005a) Turbulent shear stress profiles in a horizontal bubbly channel flow. In: Proceedings of 6th international symposium on smart control of turbulence 2005, Tokyo, 289–295

Murai Y, Sasaki T, Ishikawa M, Yamamoto F (2005b) Bubble-driven convection around cylinders confined in a channel. J Fluids Eng 127:117–123

Murai Y, Fujii H, Tasaka Y, Takeda Y (2006a) Turbulent bubbly channel flow investigated by ultrasound velocity profiler. J Fluid Sci Technol 1:12–23

Murai Y, Oishi Y, Takeda Y, Yamamoto F (2006b) Turbulent shear stress profiles in a bubbly channel flow assessed by particle tracking velocimetry. Exp Fluids 41:343–352

Murai Y, Qu JW, Yamamoto F (2006c) Three dimensional interaction of bubbles at intermediate Reynolds numbers. Multiph Sci Technol 18:175–197

Murai Y, Fukuda H, Oishi Y, Kodama Y, Yamamoto F (2007) Skin friction reduction by large air bubbles in a horizontal channel flow. Int J Multiph Flow 33:147–163

Murai Y, Oiwa H, Takeda Y (2008) Frictional drag reduction in bubbly Couette-Taylor flow. Phys Fluids 20:034101

Murai Y, Ohta S, Shigetomi A, Tasaka Y, Takeda Y (2009) Development of an ultrasonic void fraction profiler. Meas Sci Technol 20:114003

Murai Y, Tasaka Y, Nambu Y, Takeda Y, Gonzalez SR (2010) Ultrasonic detection of moving interfaces in gas–liquid two-phase flow. Flow Meas Instrum 21:356–366

Narayanan C, Lakehal D (2003) Mechanism of particle deposition in a fully developed turbulent open channel flow. Phys Fluids 15:763–775

Oishi Y, Murai Y (2014) Horizontal turbulent channel flow interacted by a single large bubble. Exp Therm Fluid Sci 55:128–139

Oishi Y, Murai Y, Tasaka Y, Takeda Y (2009) Frictional drag reduction by wavy advection of deformable bubbles. J Phys Conf Ser 147:012020

Ojima S, Hayashi K, Hosokawa S, Tomiyama A (2014) Distribution of void fraction and liquid velocity in air-water bubble column. Int J Multiph Flow 1–11. doi:10.1016/j.ijmultiphaseflow.2014.05.008

Ortiz-Villafuerte J, Hassan YA (2006) Investigation of microbubble boundary layer using particle tracking velocimetry. J Fluids Eng 128:507–519

Ouellette NT (2012) Turbulence in two dimensions. Phys Today 68–69

Pang MJ, Wei JJ, Yu B (2013) Numerical study on modulation of microbubbles on turbulence frictional drag in a horizontal channel. Ocean Eng 81:58–68

Park HJ, Oishi Y, Tasaka Y, Murai Y, Takeda Y (2009) Turbulent shear control with oscillatory bubble injection. J Phys Conf Ser 147:012037

Park HJ, Tasaka Y, Murai Y, Oishi Y (2014) Vortical structures swept by a bubble swarm in turbulent boundary layers. Chem Eng Sci 116:486–496

Piomelli U, Yuan J (2013) Numerical simulation of spatially developing, accelerating boundary layer. Phys Fluids 25:101304

Poreh M, Cermak JE (1964) Study of diffusion from a line source in a turbulent boundary layer. Int J Heat Mass Transf 7:1083–1095

Prasser HM, Scholz D, Zippe C (2001) Bubble size measurement using wire-mesh sensors. Flow Meas Instrum 12:299–312

Prosperetti A (2012) Linear oscillations of constrained drops, bubbles, and plane liquid surfaces. Phys Fluids 24:032109

Rensen J, Luther S, de Vries J, Lohse D (2005a) Hot-film anemometry in bubbly flow I: bubble–probe interaction. Int J Multiph Flow 31:285–301

Rensen J, Luther S, Lohse D (2005b) The effect of bubbles on developed turbulence. J Fluid Mech 538:153–187

Richter S, Aritomi M, Prasser HM, Humpel R (2002) Approach towards spatial phase reconstruction in transient bubbly flow using a wire-mesh sensor. Int J Heat Mass Transf 45:1063–1075

Robinson SK (1991) Coherent motions in the turbulent boundary layer. Annu Rev Fluid Mech 23:601–639

Ronen D (1982) The effect of oil price on the optimal speed of ships. J Oper Res 33:1035–1040

Rust AC, Manga M (2002a) Effects of bubble deformation in the viscosity of dilute suspensions. J Non-Newton Fluid Mech 104:53–63

Rust AC, Manga M (2002b) Bubble shapes and orientations in low Re simple shear flow. J Colloid Interface Sci 249:476–480

Ryskin G, Leal LG (1984) Numerical solution of free-boundary problems in fluid mechanics: part 1 the finite-difference technique. J Fluid Mech 148:1–17

Sakurai K, Tasaka Y, Murai Y (2013) Modification of effective viscosity on bubbly flows due to transient bubble deformation. Trans. Japan Soc. Mech. Eng., Ser. B, 79: 1–11 (in Japanese). English version of similar contents: Murai Y, Tasaka Y, Sakurai K, Oyama K, Takeda Y (2010) Ultrasound Doppler rheometry from spin response of viscoelastic and bubbly Liquids. In: Proceedings 7th international symposium on ultrasonic Doppler methods, Gothenburg, Sweden, 9–12

Sanders WC, Winkel ES, Dowling DR, Perlin M, Ceccio SL (2006) Bubble friction drag reduction in a high-Reynolds-number flat-plate turbulent boundary layer. J Fluid Mech 552:353–380

Sangani AS, Didwania AK (1993) Dynamic simulations of flows of bubbly liquids at large Reynolds numbers. J Fluid Mech 250:307–337

Sangani AS, Kang SY, Tsao HK, Koch DL (1997) Rheology of dense bubble suspensions. Phys Fluids 9(6):1540–1561

Schowalter WR, Chaffey CE, Brenner H (1968) Rheological behavior of a dilute emulsion. J Colloid Interface Sci 26:152–160

Seo JH, Lele SK, Tryggvason G (2010) Investigation and modeling of bubble–bubble interaction effect in homogeneous bubbly flows. Phys Fluids 22:063302

Serizawa A, Kataoka I (1990) Turbulence suppression in bubbly two-phase flow. Nuclear Eng Des 122:1–16

Serizawa A, Inui T, Eguchi T (2005) Flow characteristics and pseudo-laminarization of vertically upward air–water milky bubbly flow with micro bubbles in a pipe. Jpn J Multiph Flow 19:335–340 (in Japanese)

Shen X, Ceccio S, Perlin M (2006) Influence of bubble size on micro-bubble drag reduction. Exp Fluids 41:415–424

Shiomi Y, Kutsuna H, Akagawa K, Ozawa M (1993) Two-phase flow in an annulus with a rotating inner cylinder (flow pattern in bubbly flow region). Nuclear Eng Des 141:27–34

So S, Morikita H, Takagi S, Matsumoto Y (2002) Laser Doppler velocimetry measurement of turbulent bubbly channel flow. Exp Fluids 33:135–142

Stickel J, Powell RL (2005) Fluid mechanics and rheology of dense suspensions. Annu Rev Fluid Mech 37:129–149

Stutz B, Legoupil S (2003) X-ray measurements within unsteady cavitation. Exp Fluids 35(2):130–138

Sugiyama K, Calzavarini E, Lohse D (2008) Microbubbly drag reduction in Taylor–Couette flow in wavy vortex regime. J Fluid Mech 608:21–41

Takagi S, Matsumoto Y (2011) Surfactant effects on bubble motion and bubbly flow. Annu Rev Fluid Mech 43:615–636

Takagi S, Ogasawara T, Fukuta M, Matsumoto Y (2009) Surfactant effect on the bubble motions and bubbly flow structures in a vertical channel. Fluid Dyn Res 41:065003

Takahashi T, Kakugawa A, Makino M, Kodama Y (2003) Experimental study on scale effect of drag reduction by microbubbles using very large flat plate ships. J Kansai Soc Nav Archit Jpn 239:11–20 (in Japanese)

Takeda Y (2012) Ultrasonic Doppler velocity profiler for fluid flow. Fluid mechanics and its applications, Ser. 101, Springer, Berlin

Takeda Y, Fischer WE, Sakakibara J (1994) Decomposition of the modulated waves in a rotating Couette system. Science 263:502–505

Tanaka M (2013) Inverse transverse migration of small bubbles in turbulence. J Phys Soc Jpn 82:044401

Taniere A, Oesterle B, Monnier JC (1997) On the behavior of solid particles in a horizontal boundary layer with turbulence and saltation effects. Exp Fluids 23:463–471

Taylor GI (1923) Stability of a viscous liquid contained between two rotating cylinders. Philos Trans R Soc Lond Ser A 223:289–343

Timkin LS, Gorelik RS (2010) Specificity of laminar-turbulent transition un upward monodispersed microbubbly flow. Tech Phys Lett 36:493–495

Toschi F, Bodenschartz E (2009) Lagrangian properties of particles in turbulence. Annu Rev Fluid Mech 41:375–404

Tran-Cong S, Marie JL, Perkins RJ (2008) Bubble migration in a turbulent boundary layer. Int J Multiph Flow 34:786–807

Tsai JF, Chen CC (2011) Boundary layer mixture model for a microbubble drag reduction technique. Int Sch Res Netw 2011:405701

van den Berg TH, Luther S, Lathrop DP, Lohse D (2005) Drag reduction in bubbly Taylor–Couette turbulence. Phys Rev Lett 94:044501

van den Berg TH, Luther S, Lathrop D, Lohse D (2007) Bubbly turbulent drag reduction is a boundary effect. Phys Rev Lett 98:084501

van Gils DPM, Guzman DN, Sun C, Lohse D (2013) The importance of bubble deformability for strong drag reduction in bubbly turbulent Taylor–Couette flow. J Fluid Mech 722:317–347

Warsito W, Fan LS (2001) Measurement of real-time flow structures in gas–liquid and gas–liquid–solid flow systems using electrical capacitance tomography (ECT). Chem Eng Sci 56:6455–6462

Watamura T, Tasaka Y, Murai Y (2013) Intensified and attenuated waves in a microbubble Taylor-Couette flow. Phys Fluids 25:054107

Watanabe O, Masuko A, Shirose Y (1998) Measurements of drag reduction by microbubbles using very long ship models. J Soc Nav Archit Jpn 183:53–63

Winkel ES, Ceccio SL, Dowling DR, Perlin M (2004) Bubble-size distributions produced by wall injection of air into flowing fresh water, saltwater and surfactant solutions. Exp Fluids 37:802–810

Wronski S, Hubacz R, Ryszczuk T (2005) Interfacial area in a reactor with helicoidal flow for the two-phase gas–liquid system. Chem Eng J 105:71–79

Wu SJ, Hsu CH, Lin TT (2007) Model test of the surface and submerged vehicles with the micro-bubble drag reduction. Ocean Eng 34:83–93

Wu SJ, Ouyang K, Shiah SW (2008) Robust design of microbubble drag reduction in a channel flow using the Taguchi method. Ocean Eng 35:856–863

Xu J, Maxey ML, Karniadakis GE (2002) Numerical simulation of turbulent drag reduction using micro-bubbles. J Fluid Mech 468:271–281

Yoshida K, Tasaka Y, Murai Y, Takeda Y (2009) Mode transition in bubbly Taylor–Couette flow measured by PTV. J Phys Conf Ser 147:012013

Zenit R, Koch D, Sangani AS (2001) Measurements of the average properties of a suspension of bubbles rising in a vertical channel. J Fluid Mech 429:307–342

Zhang DZ, Prosperetti A (1994) Averaged equations for inviscid disperse two-phase flow. J Fluid Mech 267:185–219

Zhao LH, Andersson HI, Gillissen JJJ (2010) Turbulence modulation and drag reduction by spherical particles. Phys Fluids 22:081702

Zhao LH, Marchioli C, Andersson HI (2012) Stokes number effects on particle slip velocity in wall-bounded turbulence and implications for dispersion models. Phys Fluids 24:021705

Zhen L, Hassan YA (2006) Wavelet autocorrelation identification of the turbulent flow multi-scales for drag reduction process in microbubbly flows. Chem Eng Sci 61:7107–7114

Zhen N, Handler RA, Zhang Q, Oeth C (2013) Evolution of a hairpin vortex in a shear-thinning fluid governed by a power-law model. Phys Fluids 25:110703